Hindawi
Shock and Vibration
Volume 2019, Article ID 6362198, 24 pages
https://doi.org/10.1155/2019/6362198

Research Article

Modeling and Dynamic Behavior Analysis of Rope-Guided Traction System with Terminal Tension Acting on Compensating Rope

Lei Wang,[1,2] **Guohua Cao**,[1,2] **Naige Wang**,[1,2] **and Lu Yan**[1,2]

[1]*School of Mechatronic Engineering, China University of Mining and Technology, Xuzhou 221116, China*
[2]*Jiangsu Key Laboratory of Mine Mechanical and Electrical Equipment, China University of Mining and Technology, Xuzhou 221116, China*

Correspondence should be addressed to Guohua Cao; caoguohua@cumt.edu.cn

Received 22 January 2019; Revised 10 April 2019; Accepted 19 May 2019; Published 18 June 2019

Academic Editor: Jean-Jacques Sinou

Traction systems are a good choice for high-rise lift systems, especially in deep wells. With increasing lift depth and weight, rope-guided traction systems have become an essential design methodology in the mine lift field. In this paper, a comprehensive mathematical model is established to simulate the dynamical responses of a rope-guided traction system with different terminal tensions acting on the compensating rope. The results and analysis presented in this paper reveal dynamical responses in terms of longitudinal and transverse vibration. Additionally, a wide range of resonances occurs in the target system. Differences in the dynamical responses between a traditional traction system and tensioned traction system are analysed in detail. Through comparison and analysis, it is determined that terminal tension plays an important role in the suppression of longitudinal vibration in a system. However, changes in the amplitude of longitudinal vibration are independent of terminal tension, which only affects longitudinal elastic elongation and does not affect the basic shape of longitudinal and transverse vibrations. Based on this analysis, it can be concluded that longitudinal vibration suppression can be achieved by applying proper tension on the compensating rope to ensure that it reaches a tensioning state. Continuing to increase terminal tension is not beneficial for the vibration suppression of a system. The results presented in this paper will serve as a valuable guide for the design and optimisation of traction systems.

1. Introduction

Because of their ability to resist relatively large axial loads, ropes have been widely applied in lift systems, such as mobile cranes [1], elevators [2], and mine lifts [3]. Considering the characteristics of heavy loads and space saving, traction systems are a good choice in high-rise lift systems, especially in deep wells. With increasing lift depth, rope-guided traction systems have become a popular solution in the mine lift field. Compared to rigid guides, rope guides are easier to install and more cost-effective. Therefore, rope-guided traction systems will gradually replace traditional traction systems, meaning a dynamic model must be established to explore the dynamic characteristics of such systems.

Traditional traction systems consist of five main components: a drum, lifting rope, rigid guides, conveyance, and compensating rope. The dynamical responses of traditional lift systems have been thoroughly studied by many scholars. For example, Kimura et al.[4] established a transverse vibration model for elevators and used a single-degree-of-freedom system to analyse dynamical responses.

It is widely understood that the longitudinal and transverse vibrations of the lifting and compensating ropes are induced by excitations in the winding process of the drum. When the frequency of excitation matches the natural frequency of the system, resonance will occur at the corresponding point. This phenomenon causes impact loads during the lifting process, leading to poor stability of the system, and has been studied by many researchers for

decades. For example, Kaczmarczyk [5, 6] established longitudinal and transverse models for a catenary-vertical lifting cable system with periodic excitation to analyse passage through resonances based on a multiscale method.

Regarding continuous dynamic modelling methods, there are three main types of methods: Lagrange principle methods, Hamilton principle methods, and finite element methods (FEMs). For example, Ren and Zhu [7, 8] developed a spatial discretisation and substructure method to calculate the dynamic responses of a one-rope system with a time-varying length parameter accurately using the Lagrange equation. They also explored the longitudinal and transverse vibrations of a moving two-cable, one-rigid-body car system, where the rotation of the car was considered. Bao et al. [9] established a dynamic model for elevator lift systems based on the Hamilton principle and analysed the influence of different system parameters on transverse and longitudinal vibrations, as well as the energy characteristics of longitudinal and transverse vibrations, which were verified experimentally. Wang et al. [10] introduced an FEM to investigate the three-dimensional underwater vibrations of a geometrically nonlinear cable with a weight at the lower end. Wang [11] established a longitudinal vibration model based on the Lagrange equation for a parallel lift system with a tension auto-balance device (TABD) attached to the ends of all lifting ropes. The results revealed that for a parallel lifting system with a TABD attached to the ends of all lifting ropes, conveyance provides the main excitation that affects the longitudinal vibration of the ropes.

One can see that most previous studies on the dynamical responses of traction systems have focused on rigid guides. Rigid guides and flexible guides exhibit significant differences in terms of their dynamic responses. Several scholars have studied different types of guides and derived many meaningful results. Yang et al. [12, 13] considered the conveyance and guiding rope as a cohesive system based on dynamic analysis of the swing of the conveyance. The swing angle of the conveyance during the lifting process was obtained through numerical calculations. The influence of the length of the guiding rope, pretension of the guiding rope, lifting speed, horizontal torque, and inertia and size of the conveyance on the swing angle was analysed. Sai [14–16] analysed the reasons for the transverse vibration of a lift bucket and determined that the main internal factors leading to oscillation were the twisting force of the lifting rope, jumping of the lifting rope when the drum ran out of rope, periodic fluctuation of the lifting rope caused by errors in processing and installation, and initial offset and large acceleration of the lifting rope. The pretension of the flexible guiding rope was an important external factor affecting oscillation. The influence of the lifting weight, tension of the guiding rope, depth of the well, and lifting speed on the swing angle of the conveyance was also analysed. It was concluded that the roundness of the pulley is proportional to the swing angle of the conveyance. This roundness has the greatest influence on the swing angle and is the fundamental cause of swinging. To transform the equivalent mass and time-varying stiffness of the guiding rope to the end of the lifting rope, Cao [17] established a lateral and torsional vibration model for a rope-guided lift system and analysed the effects of various parameters on the lateral and torsional vibrations of the conveyance. It was determined that appropriate tension and distance differences can decrease the maximum lateral displacement. Considering guiding and lifting ropes as continuums, Wang et al. [18] established equations of motion for a rope-guided lifting system using first-order Lagrange equations. The geometric relationships between the conveyance and cables were accounted for by the Lagrangian multiplier. The dynamical responses of the conveyance were calculated, and the transverse displacements of the guiding ropes and constraining forces at the interfaces were obtained. He also established equations of motion using Hamilton's principle and obtained boundary conditions to calculate natural frequencies with a modified velocity of wave propagation. According to Lyapunov's second method, the rate of change in energy indicates that a cable-guided lifting system experiences stability and instability during downward and upward movements, respectively. Wang et al. [19] also considered the guiding rope as a continuum to obtain the vibration characteristics of a flexible steering lift system under multiple disturbances and proposed an adaptive transverse vibration control method.

In most previous models, the compensating rope has been considered in a free state. Few scholars have also added a compensation pulley to the end of the compensation rope to control the dynamical response of the compensation rope. For example, Crespo et al. [20] established a comprehensive mathematical model for a high-rise elevator system considering the combined lateral stiffness of the roller guides and guide rails. The results and analysis presented in his paper reveal frequency curve veering phenomena and a wide range of resonances that occur in the system. Otosuki et al. [21] presented a method of vibration control for an elevator rope based on a nonstationary sliding mode control method using an input device with gaps. The results indicated effective vibration suppression and high robustness in the cases described above, except for the case with varying parameters. Using the Hamilton principle, Bao et al. [22] established a model for the vibration control of a high-speed elevator system with a tensioned compensation rope and considered a high-speed elevator lift system as an example to simulate and analyse the model.

Overall, previous studies have largely focused on traditional lift systems. They have not accounted for the characteristics of rope guides, tensioned compensating ropes, etc., which are crucial for extreme lift depths. Additionally, previous studies have not presented any unified or comprehensive models. This paper extends the analysis presented in previous publications to develop a comprehensive mathematical model for rope-guided traction systems to analyse the dynamical behaviours of the lifting rope, compensating rope, guiding rope, and conveyance. Furthermore, comparisons of longitudinal and transverse vibrations between traditional and tensioned traction systems are presented in this paper. It is demonstrated that longitudinal vibrations in a system can be suppressed to a certain extent by applying tension to the end of the compensation

rope. In this paper, a first-order Lagrange equation is used to derive a mathematical model. The complex constraint conditions between the conveyance and ropes are derived using a condensational method. The results will serve as a helpful guide for the design and optimisation of traction systems, especially in the prediction of resonance zones and suppression of longitudinal vibrations.

2. Model Description

First, the following assumptions must be considered:

(1) The linear densities of the lifting, guiding, and compensating ropes are assumed to be uniform

(2) The bending stiffness of rope was neglected in this study

(3) Considering the small axial excitation of the friction drum, out-of-plane transverse responses relative to the ropes and conveyance are neglected

As shown in Figure 1, a rope-guided traction system consists of four main parts: the driving drum, guiding ropes, lifting rope, conveyance, and compensating rope. The guiding ropes are tensioned by T_{b_i}, $i = 1, 2$. The compensating rope is tensioned by F_T. Based on the consistent properties of guiding ropes on each side, for the sake of mathematical modelling, four total guiding ropes are equivalent to one rope on each side of the conveyance. The lengths of the lifting and compensating ropes are donated as $l_i(t)$, $i = 1, 2$. Correspondingly, their velocities and accelerations can be expressed as $v_i(t)$, $i = 1, 2$ and $a_i(t)$, $i = 1, 2$, respectively. The longitudinal dynamic displacements of the lifting and compensating ropes at a position x and time t are $u_i(x, t)$, $i = 1, 2$. The transverse dynamic displacements of the lifting and compensating ropes at a position x and time t are $y_i(x, t)$, $i = 1, 2$. The longitudinal, transverse, and rotational dynamic displacements of the conveyance are donated as u_c, y_c, and θ, respectively. The transverse dynamic displacements of the guiding rope are denoted as y_{g_i}, $i = 1, 2$. $A(B)$ is the connecting point between the lifting (compensating) rope and conveyance. C_i, $i = 1, 2, 3, 4$ are the connecting points between the guiding ropes and conveyance. The centroid point of the conveyance O is used to define the coordinate frame $O - XY$. Based on the rotation and vibration displacement of the conveyance, the connecting points A, B, C_i, $i = 1, 2, 3, 4$ between the ropes and conveyance are transformed into $A', B'C_i'$, $i = 1, 2, 3, 4$. L_{guide} is the length of the guiding rope. The horizontal distance between a connecting point C_i and the conveyance centroid O is donated as l_a. The half-height of the conveyance is donated as l_b.

Based on the schematic in Figure 1, a 3D model of a traction system with terminal tension acting on the compensating rope is presented in Figure 2. The actual installation of the traction system consists of nine main parts: the driving drum, pulley, lifting rope, conveyance, compensating rope, tension actuator, auxiliary drum, guiding rope, and sensors. In Figures 2(a) and 2(b), the tension acting on the compensating rope is applied through

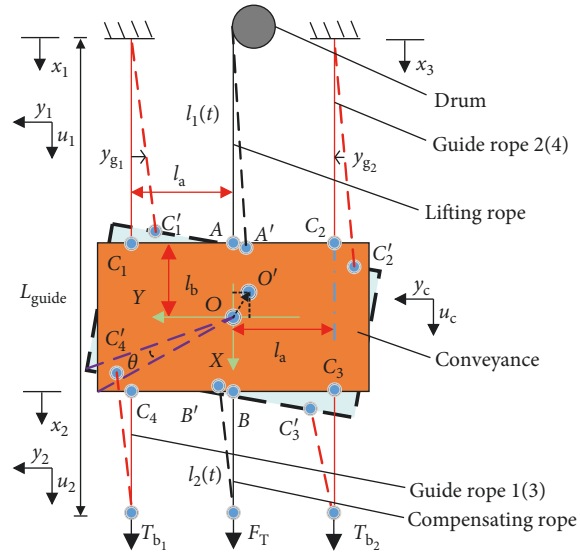

FIGURE 1: Traction system with tension acting on the compensating rope.

the electric cylinder. Using the auxiliary drum, the tensions on the compensating rope on both sides can be loaded by electric cylinders independently. Based on feedback from the tension sensor in front of the cylinder block, the tension magnitude on the compensating rope can be controlled precisely. Figures 2(c) and 2(d) present the arrangement of the conveyance and driving drum. Tension sensors are arranged on the top and bottom of the conveyance to monitor the tensions of the lifting and compensating ropes, respectively.

2.1. Mathematical Model. By considering the physical model illustrated in Figure 1, a mathematical model was established using an energy-based method. A dynamical equation for the system can be obtained by inputting the energy of the system into the first-order Lagrange equation. The kinetic energy of the system is calculated as follows:

$$
\begin{aligned}
T_k = {} & \frac{1}{2}\int_0^{l_1(t)} \rho_1 \left(\frac{Dy_1(x_1,t)}{Dt}\right)^2 dx_1 \\
& + \frac{1}{2}\int_0^{l_1(t)} \rho_1 \left(v_1 + \frac{Du_1(x_1,t)}{Dt}\right)^2 dx_1 \\
& + \frac{1}{2}\int_0^{l_2(t)} \rho_2 \left(\frac{Dy_2(x_2,t)}{Dt}\right)^2 dx_2 \\
& + \frac{1}{2}\int_0^{l_2(t)} \rho_2 \left(v_2 + \frac{Du_2(x_2,t)}{Dt}\right)^2 dx_2 + \frac{1}{2}m_c(v_1 + \dot{u}_c)^2 \\
& + \frac{1}{2}m_c\dot{y}_c^2 + \frac{1}{2}J_c\dot{\theta}^2 + \frac{1}{2}\sum_{i=1}^{2}\int_0^{L_{guide}} \rho_g \left(\frac{\partial y_{g_i}(x_3,t)}{\partial t}\right)^2 dx_3,
\end{aligned}
\tag{1}
$$

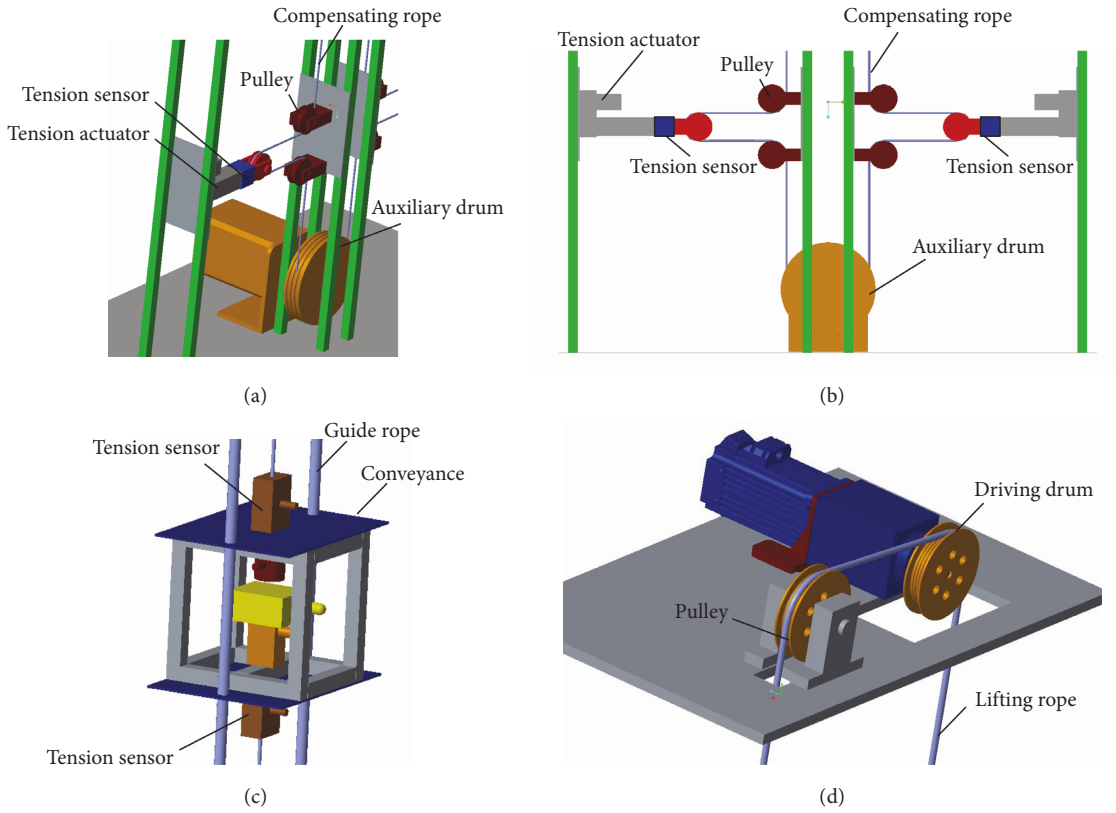

FIGURE 2: Installation schematic. The (a) system for applying tension on the compensating rope (unilateral schematic), (b) system for applying tension on the compensating rope (bilateral schematic), (c) conveyance, and (d) drum and pulley.

where x_1, x_2, and x_3 represent the coordinate measurements of the lifting rope, compensating rope, and guiding rope, respectively. As shown in Figure 1, the interval of x_1, x_2, and x_3 can be obtained as follows: $0 \le x_1 \le l_1(t)$, $0 \le x_2 \le l_2(t)$, and $0 \le x_3 \le L_{\text{guide}}$. The operator D/D$t$ represents a material derivative and is defined as follows:

$$\frac{D}{Dt} = \frac{\partial}{\partial t} + v_i \frac{\partial}{\partial x_i}, \quad i = 1, 2, \tag{2}$$

where ρ_1, ρ_2, and ρ_g are the linear densities of the lifting, compensating, and guiding ropes, respectively. m_c is the mass of the conveyance, and J_c is the moment of inertia of the conveyance.

The potential energy of the traction system is a function of vibration displacement, which is defined as follows:

$$\begin{aligned} V_e = & \int_0^{l_1(t)} \left[T_1(x_1,t)\varepsilon_1 + \frac{1}{2} EA\varepsilon_1^2 \right] dx_1 \\ & + \int_0^{l_2(t)} \left[T_2(x_2,t)\varepsilon_2 + \frac{1}{2} EA\varepsilon_2^2 \right] dx_2 \\ & + \sum_{i=1}^{2} \int_0^{L_{\text{guide}}} T_{g_i}(x_3,t)\varepsilon_{g_i} dx_3 - \int_0^{l_1(t)} \rho_1 g u_1(x_1,t) dx_1 \\ & - \int_0^{l_2(t)} \rho_2 g u_2(x_2,t) dx_2 - m_c g u_c, \end{aligned} \tag{3}$$

where EA is the axial stiffness of the ropes. $T_i(x,t)$ and $T_{g_i}(x,t)$, $i = 1, 2$ are the tensions of the ropes at a position x. Specific expressions are provided in Appendix A. ε_i, $i = 1, 2$ are the elastic strains of the ropes:

$$\begin{aligned} \varepsilon_1 &= u_{1,x}(x_1,t) + \frac{1}{2} y_{1,x}^2(x_1,t), \\ \varepsilon_2 &= u_{2,x}(x_2,t) + \frac{1}{2} y_{2,x}^2(x_2,t), \\ \varepsilon_3 &= \frac{1}{2} y_{g,x}^2(x_3,t). \end{aligned} \tag{4}$$

Based on rope damping, the dissipated energy D_e of the ropes can be calculated as follows:

$$\begin{aligned} D_e = & \frac{1}{2} \int_0^{l_1(t)} \mu_1 u_{1,t}^2(x_1,t) dx_1 + \frac{1}{2} \int_0^{l_1(t)} \mu_2 y_{1,t}^2(x_1,t) dx_1 \\ & + \frac{1}{2} \int_0^{l_2(t)} \mu_1 u_{2,t}^2(x_2,t) dx_2 + \frac{1}{2} \int_0^{l_2(t)} \mu_2 y_{2,t}^2(x_2,t) dx_2 \\ & + \frac{1}{2} \int_0^{L_{\text{guide}}} \mu_g y_{g,t}^2(x_3,t) dx_3, \end{aligned} \tag{5}$$

where μ_1, μ_2, and μ_g are the distributed damping coefficients of the lifting, compensating, and guiding ropes, respectively.

As shown in Figure 1, translation of the centroid of the conveyance can be represented as $[u_c, y_c]^T$ in the coordinate system. Using a transformation matrix, the constraint conditions for a rope-guided traction system can be obtained as follows:

$$g_z(t) = \left[\, g_1^T(t) \;\; g_2^T(t) \;\; g_3^T(t) \,\right], \tag{6}$$

where $g_1(t)$ denotes the constraint relationship between the lifting rope and conveyance, $g_2(t)$ denotes the constraint relationship between compensating rope and conveyance, and $g_3(t)$ denotes the constraint relationship between the guiding rope and conveyance. Specific expressions [20] are provided in Appendix B. Based on small rotations of the conveyance, some reasonable approximations can be implemented, namely, $\sin\theta \approx \theta$ and $\cos\theta \approx 1$. Therefore, the constraint conditions are simplified as shown in Appendix B. Considering the boundary excitation at the drum, the transverse displacement of the lifting rope can be expressed in the following form:

$$y_1(x_1,t) = \overline{y}_1(x_1,t) + \overline{h}_{y1}(x_1,t), \tag{7}$$

where $\overline{y}_1(x_1,t)$ is selected to satisfy the corresponding homogeneous boundary conditions and $\overline{h}_{y1}(x_1,t)$ compensates for the effects of boundary excitation that are not satisfied by $\overline{y}_1(x_1,t)$. Considering that excitation is linearly distributed, the distribution function of the excitation $\overline{h}_{y_1}(x_1,t)$ is defined as a first-order polynomial at a position x_1 and time t, which is expressed as follows:

$$\overline{h}_{y_1}(x_1,t) = e_y(t)\cdot\left(1 - \frac{x_1}{l_1(t)}\right). \tag{8}$$

Considering the geometric constraints of this model, the homogeneous boundary conditions at the drum, conveyance, and end of the compensating rope can be obtained as follows:

$$\begin{aligned} u_1(0,t) &= 0,\\ \overline{y}_1(0,t) &= 0,\\ y_2(l_2(t),t) &= 0. \end{aligned} \tag{9}$$

The homogeneous boundary conditions at the top and end of guiding rope can be obtained as follows:

$$\begin{aligned} y_{g_1}(0,t) &= 0,\\ y_{g_2}(0,t) &= 0,\\ y_{g_1}\left(L_{\text{guide}},t\right) &= 0,\\ y_{g_2}\left(L_{\text{guide}},t\right) &= 0. \end{aligned} \tag{10}$$

2.2. Dynamical Equations. For simplicity, two new dimensionless parameters ξ_1 and ξ_2 are introduced. The original time-varying domain $[0, l(t)]$ is transformed into a fixed domain $[0, 1]$. Therefore, the dependent variables $u_i(x_i,t)$, $\overline{y}_1(x_i,t)$, and $y_2(x_i,t)$ become $\widehat{u}_i(\xi_i,t)$ and $\widehat{y}_i(\xi_i,t)$, $i = 1, 2$. Their partial derivatives with respect to ξ_i and t will become

$$\begin{aligned} \frac{\partial Y(x_i,t)}{\partial x_i} &= \frac{1}{l_i(t)}\frac{\partial \widehat{Y}(\xi_i,t)}{\partial \xi_i},\\ \frac{\partial Y(x_i,t)}{\partial t} &= \frac{\partial \widehat{Y}(\xi_i,t)}{\partial t} + \frac{v_i(t)\xi_i}{l_i(t)}\frac{\partial \widehat{Y}(\xi_i,t)}{\partial \xi_i}, \quad i = 1,2, \end{aligned} \tag{11}$$

where $Y(x_i,t)$ is a representative of $u_i(x_i,t)$, $\overline{y}_1(x_i,t)$, and $y_2(x_i,t)$, $i = 1, 2$. $\widehat{Y}(x_i,t)$ denotes $\widehat{u}_i(\xi_i,t)$ and $\widehat{y}_i(\xi_i,t)$, $i = 1, 2$.

The dependent variable $y_{g_i}(x_3,t)$ becomes $\widehat{y}_{g_i}(\xi_3,t)$ with the introduction of ξ_3. Its partial derivatives with respect to ξ_3 and t will become

$$\begin{aligned} \frac{\partial Y(x_3,t)}{\partial x_3} &= \frac{1}{L_{\text{guide}}}\frac{\partial \widehat{Y}(\xi_3,t)}{\partial \xi_3},\\ \frac{\partial Y(x_3,t)}{\partial t} &= \frac{\partial \widehat{Y}(\xi_3,t)}{\partial t}. \end{aligned} \tag{12}$$

Accordingly, the expression of rope tension and the boundary conditions for the old variables x_i, $i = 1, 2, 3$ are transformed into a new expression for ξ_i, $i = 1, 2, 3$.

Based on the continuous characteristics of ropes, the dynamic displacement coordinates can be approximated using the assuming modal method (AMM). The AMM is a discretisation method for continuous systems. It uses a linear combination of finite modal functions to approximate the responses of the system, which consist of discrete-order and modal functions. The selection of modal functions must meet the limitations of boundary conditions. Discrete results can be obtained as follows:

$$\begin{aligned} \widehat{u}_1(\xi_1,t) &= \sum_{i=1}^{N_1}\phi_{1i}(\xi_1)q_{1i}(t),\\ \widehat{u}_2(\xi_2,t) &= \phi_{20}(\xi_2)q_{20}(t) + \sum_{i=1}^{N_1}\phi_{2i}(\xi_2)q_{2i}(t),\\ \widehat{y}_1(\xi_1,t) &= \sum_{i=1}^{N_2}\kappa_{1i}(\xi_1)r_{1i}(t),\\ \widehat{y}_2(\xi_2,t) &= \sum_{i=1}^{N_2}\kappa_{2i}(\xi_2)r_{2i}(t),\\ \widehat{y}_{g_1}(\xi_3,t) &= \sum_{i=1}^{N_3}\psi_{1i}(\xi_3)k_{1i}(t),\\ \widehat{y}_{g_2}(\xi_3,t) &= \sum_{i=1}^{N_3}\psi_{1i}(\xi_3)k_{2i}(t), \end{aligned} \tag{13}$$

where N_1 and N_2 denote the included discrete order of the lifting and compensating rope longitudinal and transverse displacements, respectively. N_3 denotes the mode number of guiding rope transverse displacement. $q_{1,i}(t), q_{2,i}(t)$, $r_{1,i}(t), r_{2,i}(t), k_{1i}(t)$, and $k_{2i}(t)$ are the generalised coordinates of the traction system. $\phi_{1i}(\xi_1), \phi_{2i}(\xi_2), k_{1i}(\xi_1)$, $k_{2i}(\xi_2), \psi_{1i}(\xi_1)$, and $\psi_{2i}(\xi_2)$ are the corresponding trial functions that satisfy the homogeneous boundary conditions

and constraint equations of the system [23]. Therefore, the trial functions can be set as follows:

$$\begin{aligned}
\phi_{1i}(\xi_1) &= \sin\left(\frac{2i-1}{2}\pi\xi_1\right),\\
\phi_{20} &= \frac{1}{2},\\
\phi_{2i}(\xi_2) &= \sqrt{2}\cos(i\pi\xi_2),\\
\kappa_{1i}(\xi_1) &= \sin\left(\frac{2i-1}{2}\pi\xi_1\right),\\
\kappa_{2i}(\xi_2) &= \cos\left(\frac{2i-1}{2}\pi\xi_2\right),\\
\psi_{1i}(\xi_3) &= \sin(i\pi\xi_3).
\end{aligned} \tag{14}$$

Here, $1 \le i \le N_i$. By substituting equation (14) into equation (13), the derivatives of the time and position variables can be obtained as follows:

$$\begin{aligned}
\widehat{W}_{i,t}(\xi,t) &= \sum_{i=1}^{N_1} A_i(\xi)\dot{p}_i(t),\\
\widehat{W}_{i,\xi_i}(\xi,t) &= \sum_{i=1}^{N_1} A_i'(\xi)p_i(t),\\
\widehat{W}_{i,tt}(\xi,t) &= \sum_{i=1}^{N_1} A_i(\xi)\ddot{p}_i(t),\\
\widehat{W}_{i,\xi_i\xi_i}(\xi,t) &= \sum_{i=1}^{N_1} A_i''(\xi)p_i(t),\\
\widehat{W}_{i,\xi_i t}(\xi,t) &= \sum_{i=1}^{N_1} A_i'(\xi)\dot{p}_i(t),
\end{aligned} \tag{15}$$

where $\widehat{W}_i(\xi,t)$ is a representative of $\widehat{u}_1(\xi_1,t), \widehat{u}_2(\xi_2,t)$, $\widehat{y}_1(\xi_1,t), \widehat{y}_2(\xi_2,t), \widehat{y}_{g_1}(\xi_3,t)$, and $\widehat{y}_{g_2}(\xi_3,t)$. $A_i(\xi)$ is a representative of $\phi_{1i}(\xi_1), \phi_{2i}(\xi_2), \kappa_{1i}(\xi_1), \kappa_{2i}(\xi_2), \psi_{1i}(\xi_1)$, and $\psi_{2i}(\xi_2)$. $p_i(t)$ is a representative of $q_{1,i}(t), q_{2,i}(t), r_{1,i}(t)$, $r_{2,i}(t), k_{1i}(t)$, and $k_{2i}(t)$.

By substituting equation (15) into equations (1), (3), and (5), the discretised kinetic energy and potential energy are introduced into the first-order Lagrange equation.

$$\frac{d}{dt}\left(\frac{\partial T_{\mathrm{k}}}{\partial \dot{q}_j}\right) - \frac{\partial K_{\mathrm{e}}}{\partial q_j} + \frac{\partial D_{\mathrm{e}}}{\partial \dot{q}_j} + \frac{\partial E_{\mathrm{e}}}{\partial q_j} = Q_j + \sum_{k=1}^{n}\lambda_k\frac{\partial g_k}{\partial q_j}. \tag{16}$$

A dynamical equation for the system can be obtained as follows:

$$\begin{cases}
\mathbf{M}(t)\ddot{\mathbf{q}}(t) + \mathbf{C}(t)\dot{\mathbf{q}}(t) + \mathbf{K}(t)\mathbf{q}(t) = \mathbf{F}(t) + \mathbf{N}(t) + \mathbf{G}^{\mathrm{T}}\boldsymbol{\lambda},\\
\mathbf{g}_{\mathbf{z}}(\mathbf{q},t) = 0,
\end{cases} \tag{17}$$

where $\mathbf{M}(t), \mathbf{C}(t), \mathbf{K}(t)$, and $\mathbf{F}(t)$ are the mass, damping, stiffness, and force matrices, respectively. $\mathbf{N}(t)$ is the coupling term introduced by the interaction between transverse and longitudinal vibrations. The entries in the matrices, force vectors, and specific forms of the elements in the matrices are presented in Appendix C.

Here, $\mathbf{q} = (k_{11},\ldots,k_{1N_3},k_{21},\ldots,k_{2N_3},q_{11},\ldots,q_{1N_1},q_{20},$ $q_{21},\ldots,q_{2N_1},r_{11},\ldots,r_{1N_2},r_{21},\ldots,r_{2N_2},q_{c_1},q_{c_2},q_{c_3})^{\mathrm{T}}$ is the vector of generalised coordinates. The conveyance displacements u_{c}, y_{c}, and θ are denoted as q_{c_1}, q_{c_2}, and q_{c_3}, respectively. $\mathbf{g}_{\mathbf{z}}$ represents the constraint equations. $\mathbf{G} = \partial\mathbf{g}_{\mathbf{z}}(t)/\partial\mathbf{q}$ is a Jacobian matrix of the constraint equations. $\boldsymbol{\lambda} = [\lambda_1,\lambda_2,\ldots,\lambda_8]$ are Lagrangian multipliers that denote constraint forces between the ropes and conveyance.

2.3. Numerical Calculation. As shown in equation (17), the governing equation for the system is a mixed-differential-algebraic equation. Here, a substructure method is introduced to eliminate the Lagrange multipliers. First, the Jacobian matrix of constraint equations for the generalised coordinates is divided into two parts as follows:

$$\mathbf{G}(t) = [\,\mathbf{G}_0 \;\; \mathbf{G}_1\,], \tag{18}$$

where $\mathbf{G}_0$ must be a nonsingular $C \times C$ matrix and C is the number of constraint equations. Here, a coordinate transformation matrix $\mathrm{T_r}$ is introduced to adjust the order of generalised coordinates to ensure that $\mathbf{G}_0$ is nonsingular:

$$\widetilde{\mathbf{p}} = \mathrm{T_r}\cdot\mathbf{q}, \tag{19}$$

where $\widetilde{\mathbf{p}}$ is the new generalised coordinate vector. The matrices $\mathbf{M}(t), \mathbf{C}(t), \mathbf{K}(t), \mathbf{F}(t)$, and $\mathbf{N}(t)$ are transformed as follows:

$$\begin{aligned}
\widetilde{\mathbf{M}}(t) &= \mathrm{T_r}\mathbf{M}(t)\mathrm{T_r^T},\\
\widetilde{\mathbf{C}}(t) &= \mathrm{T_r}\mathbf{C}(t)\mathrm{T_r^T},\\
\widetilde{\mathbf{K}}(t) &= \mathrm{T_r}\mathbf{K}(t)\mathrm{T_r^T},\\
\widetilde{\mathbf{F}}(t) &= \mathrm{T_r}[\mathbf{F}(t) + \mathbf{N}(t)],\\
\widetilde{\mathbf{G}} &= \mathbf{G}\mathrm{T_r^T} = \left[\,\widetilde{\mathbf{G}}_0 \;\; \widetilde{\mathbf{G}}_1\,\right].
\end{aligned} \tag{20}$$

Therefore, the dynamical equation for the system is transformed as follows:

$$\begin{cases}
\widetilde{\mathbf{M}}(t)\ddot{\widetilde{\mathbf{p}}} + \widetilde{\mathbf{C}}(t)\dot{\widetilde{\mathbf{p}}} + \widetilde{\mathbf{K}}(t)\widetilde{\mathbf{p}} = \widetilde{\mathbf{F}}(t) + \widetilde{\mathbf{G}}^{\mathrm{T}}\widetilde{\boldsymbol{\lambda}},\\
\mathbf{g}_{\mathbf{z}}(\widetilde{\mathbf{p}},t) = \mathbf{0}.
\end{cases} \tag{21}$$

The constraint conditions can be written as

$$\mathbf{g}_{\mathbf{z}}(\widetilde{\mathbf{p}},t) = \widetilde{\mathbf{G}}(t)\widetilde{\mathbf{p}} + \mathbf{g}_{\mathbf{r}}(t) = 0. \tag{22}$$

Suppose

$$\begin{aligned}
\widetilde{\mathbf{G}}(t) &= \left[\,\widetilde{\mathbf{G}}_0 \;\; \widetilde{\mathbf{G}}_1\,\right],\\
\widetilde{\mathbf{p}} &= \left[\,\widetilde{\mathbf{p}}_0 \;\; \widetilde{\mathbf{p}}_1\,\right]^{\mathrm{T}}.
\end{aligned} \tag{23}$$

Then, the constraint equations can be written as

$$\mathbf{g}_{\mathbf{z}}(\mathbf{p},t) = \left[\widetilde{\mathbf{G}}_0\,\widetilde{\mathbf{G}}_1\right]\cdot\left[\widetilde{\mathbf{p}}_0\,\widetilde{\mathbf{p}}_1\right]^{\mathrm{T}} + \mathbf{g}_{\mathbf{r}}(t) = 0 \tag{24}$$

In this situation, $\mathbf{g}_{\mathbf{r}}(t) = 0$. By solving equation (24), the generalised coordinates $\widetilde{\mathbf{p}}$ can be written as

$$\widetilde{\mathbf{p}} = \begin{bmatrix} -\widetilde{\mathbf{G}}_0^{-1}\widetilde{\mathbf{G}}_1 \\ \mathbf{I} \end{bmatrix} \widetilde{\mathbf{p}}_1, \tag{25}$$

where $\widetilde{\mathbf{p}}_1$ is a vector that is linearly independent and $\mathbf{I}$ is an identity matrix.

Suppose

$$\mathbf{U}(t) = \begin{bmatrix} -\widetilde{\mathbf{G}}_0^{-1}\widetilde{\mathbf{G}}_1 \\ \mathbf{I} \end{bmatrix}. \tag{26}$$

Then, differentiating equation (25) once and twice yields

$$\begin{aligned} \widetilde{\mathbf{p}} &= \mathbf{U}(t)\widetilde{\mathbf{p}}_1, \\ \dot{\widetilde{\mathbf{p}}} &= \dot{\mathbf{U}}(t)\widetilde{\mathbf{p}}_1 + \mathbf{U}(t)\dot{\widetilde{\mathbf{p}}}_1, \\ \ddot{\widetilde{\mathbf{p}}} &= \ddot{\mathbf{U}}(t)\widetilde{\mathbf{p}}_1 + 2\dot{\mathbf{U}}(t)\dot{\widetilde{\mathbf{p}}}_1 + \mathbf{U}(t)\ddot{\widetilde{\mathbf{p}}}_1. \end{aligned} \tag{27}$$

Substituting equation (27) into equation (21) and premultiplying by $\mathbf{U}^{\mathrm{T}}(t)$ yields

$$\overline{\mathbf{M}}(t)\ddot{\widetilde{\mathbf{p}}}_1 + \overline{\mathbf{C}}(t)\dot{\widetilde{\mathbf{p}}}_1 + \overline{\mathbf{K}}(t)\widetilde{\mathbf{p}}_1 = \overline{\mathbf{F}}(t). \tag{28}$$

Here, by using $\mathbf{U}^{\mathrm{T}}\widetilde{\mathbf{G}}^{\mathrm{T}} = 0$, the generalised mass, stiffness, and damping matrices are transformed as follows:

$$\begin{aligned} \overline{\mathbf{M}}(t) &= \mathbf{U}^{\mathrm{T}}\widetilde{\mathbf{M}}(t)\mathbf{U}, \\ \overline{\mathbf{C}}(t) &= 2\mathbf{U}^{\mathrm{T}}\widetilde{\mathbf{M}}(t)\dot{\mathbf{U}} + \mathbf{U}^{\mathrm{T}}\widetilde{\mathbf{C}}(t)\mathbf{U}, \\ \overline{\mathbf{K}}(t) &= \mathbf{U}^{\mathrm{T}}\widetilde{\mathbf{M}}(t)\ddot{\mathbf{U}} + \mathbf{U}^{\mathrm{T}}\widetilde{\mathbf{C}}(t)\dot{\mathbf{U}} + \mathbf{U}^{\mathrm{T}}\widetilde{\mathbf{K}}(t)\mathbf{U}, \\ \overline{\mathbf{F}}(t) &= \mathbf{U}^{\mathrm{T}}\widetilde{\mathbf{F}}(t). \end{aligned} \tag{29}$$

By eliminating the Lagrange multipliers, the differential-algebraic equations are transformed into ordinary differential equations (ODEs). The above ODEs can be solved using numerical methods, meaning the dynamical responses of the traction system can be obtained.

3. Dynamical Responses

To obtain dynamical responses, numerical simulations were applied to the rope-guided traction system. The typical parameters for a traction system with tension on the compensating rope are defined as follows: $\rho_1 = 23.6\,\mathrm{kg/m}$, $\rho_2 = 23.6\,\mathrm{kg/m}$, $\rho_g = 28.3\,\mathrm{kg/m}$, $m_c = 45000\,\mathrm{kg}$, $J_P = 8.56\mathrm{e}4\,\mathrm{kg}\cdot\mathrm{m}^2$, $L_{\mathrm{guide}} = 1200\,\mathrm{m}$, $l_a = 1.8\,\mathrm{m}$, $l_b = 7.5\,\mathrm{m}$, and $EA = 4\mathrm{e}8\,\mathrm{N}$. The initial and final lengths of the lifting rope are 1150 m and 70 m, respectively. The dynamical responses of the traction system are discussed below. The displacement, velocity, and acceleration profiles of the conveyance are presented in Figure 3.

In equation (17), one can see that the coupling term $\mathbf{N}(t)$ for the longitudinal and transverse vibrations will participate in the dynamical equation for the system as a separate term. Using numerical solution methods, the dynamical responses can be obtained as described below.

3.1. Longitudinal Response. First, the longitudinal vibration of the system is obtained as follows. To explore the effects of terminal tension on the longitudinal vibration of the system, the gravitational potential energy of the lift system is ignored. The natural frequency of longitudinal vibration (red line) and frequency of excitation (blue line) are presented in Figure 4.

Here, a traction system with a terminal tension of $F_T = 5\times10^4\,\mathrm{N}$ was selected as an example. The longitudinal response consists of two parts: vibration displacement caused by inertia and stiffness and elastic elongation caused by terminal tension. To observe the characteristics of longitudinal vibration clearly, these parts must be separated. For example, the longitudinal response of the conveyance with terminal tension acting on the compensating rope is presented in Figure 5(a). This longitudinal response is divided into vibration displacement, which is presented in Figure 5(b), and elastic elongation, which is presented in Figure 5(c). The distinction between vibration displacement and elastic displacement is clear.

Figure 6 presents the longitudinal responses of the traction system at the midpoint of the lifting rope, conveyance, midpoint of the compensating rope, and end point of the compensating rope. One can see a resonance region in the longitudinal vibration. At 20 s and 109 s, there are two steps in the longitudinal response caused by lift acceleration. Over time, the lifting rope becomes longer and the compensating rope becomes shorter. The stiffness of the ropes follows an opposite trend. As the stiffness of rope increases, the magnitude of the step caused by acceleration decreases. The opposite also applies. In Figure 6, it is clear that resonance occurs from time approximately 83 s to 108 s. This can be proven based on Figure 4 by observing the intersection point of the longitudinal natural frequency and excitation. Based on effects of damping, the greatest point of resonance does not appear at the intersection but is delayed. In Figure 6, the longitudinal response is an inclined vibration curve. As mentioned above, it must be separated into two parts: the vibration displacement and elastic displacement.

Based on the least squares method, the vibration displacement and elastic displacement are separated in Figures 7 and 8. Figure 7 presents the elastic elongation caused by the terminal tension acting on the compensating rope at different positions in the traction system. In the figures above, the red, blue, green, and yellow lines represent the longitudinal displacement at the midpoint of the lifting rope, conveyance, and midpoint and end point of the compensating rope, respectively. Here, one can see that the elastic elongations at different positions along the ropes are inconsistent with the constant tension acting on the compensating rope. The length of a rope is the key factor affecting its stiffness. The stiffness of ropes also varies with time in lift systems with time-varying length. As the conveyance is lifted up, the stiffness of the lifting rope increases and that of the compensating rope decreases. Based on the increasing stiffness of the lifting rope, the elastic elongation caused by the tension acting on compensating rope decreases. Overall, the elongation of the lifting rope and shortening of the compensating rope are complementary at the end of the rope. Therefore, at the end of the compensating rope, the elastic elongation is relatively steady. However, the elongation of the lifting rope and shortening of

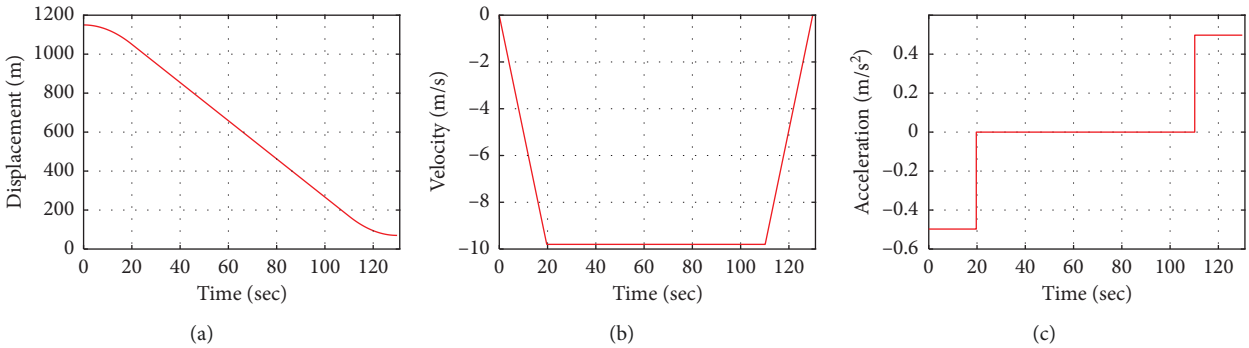

Figure 3: Conveyance movement profiles. The (a) displacement curve, (b) velocity curve, and (c) acceleration curve.

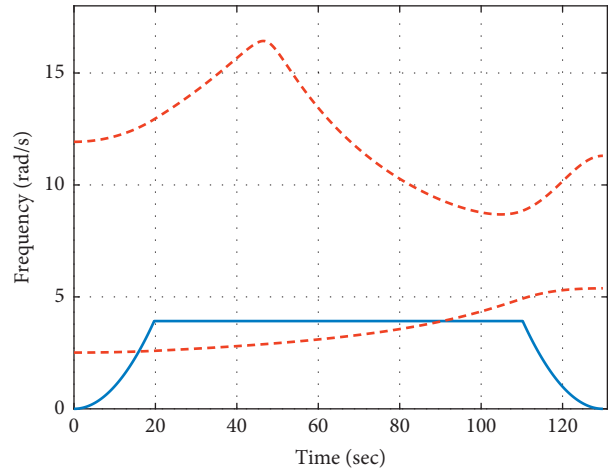

Figure 4: Natural frequency of the longitudinal vibration (red line) and frequency of excitation (blue line).

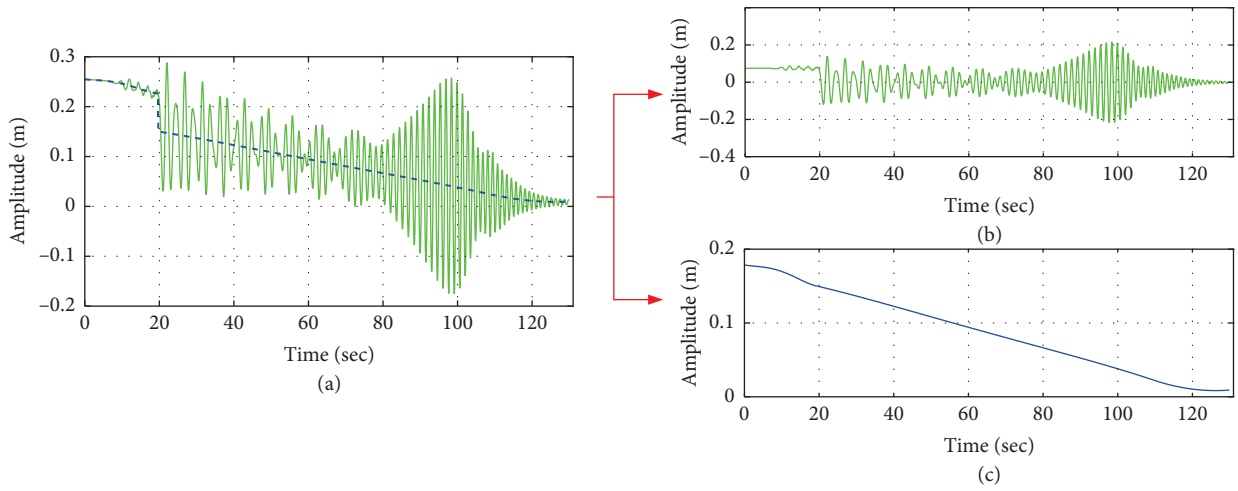

Figure 5: Separation schematic diagram of vibration displacement and elastic displacement. The (a) original signal, (b) vibration displacement, and (c) elastic displacement.

the compensating rope caused by terminal tension cannot completely compensate for each other. This is why the longitudinal trends in Figure 7 decline at the midpoints of the lifting rope, compensating rope, and conveyance. At the conveyance, the negative slope of the longitudinal trend is the largest. This means that the elastic elongation caused by terminal tension changes the most at the conveyance during the lifting process. In Figure 8, one can see that the amplitude of longitudinal vibration increases with the observation points of the traction system from the top to the end. At the end point of the compensating rope, the amplitude reaches a maximum. Based on this phenomenon, one can see

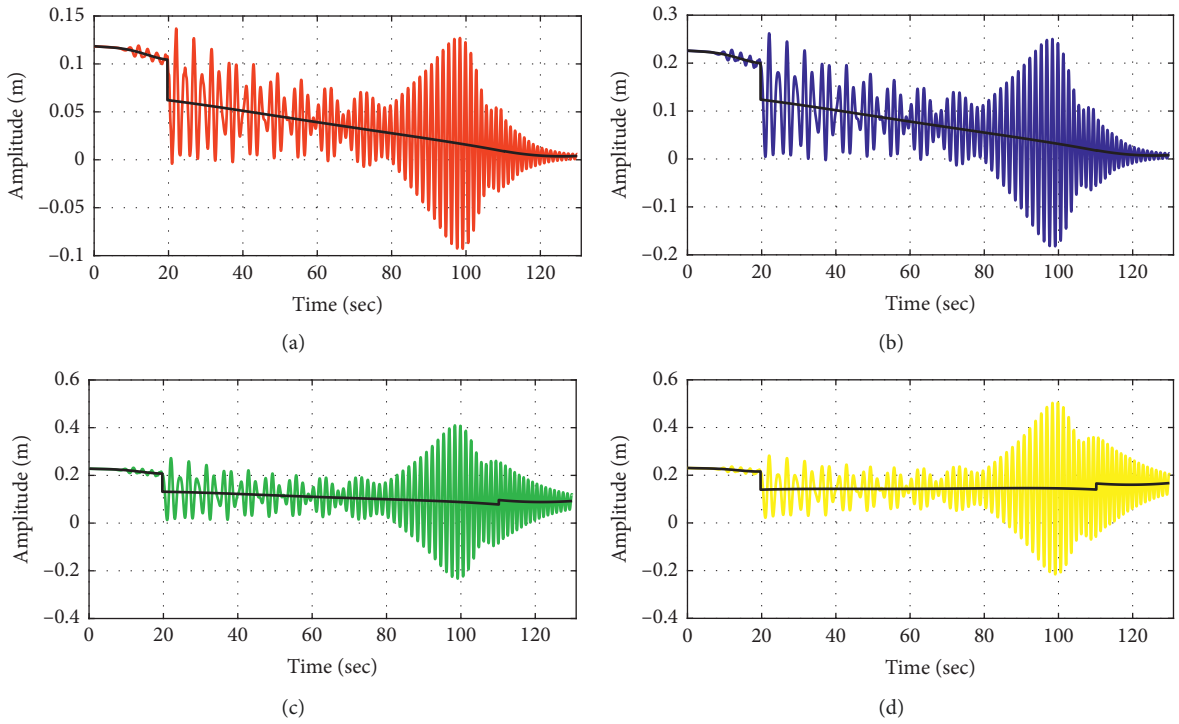

Figure 6: Longitudinal responses of the traction system at different positions. The (a) midpoint of the lifting rope, (b) conveyance, (c) midpoint of the compensating rope, and (d) end point of the compensating rope.

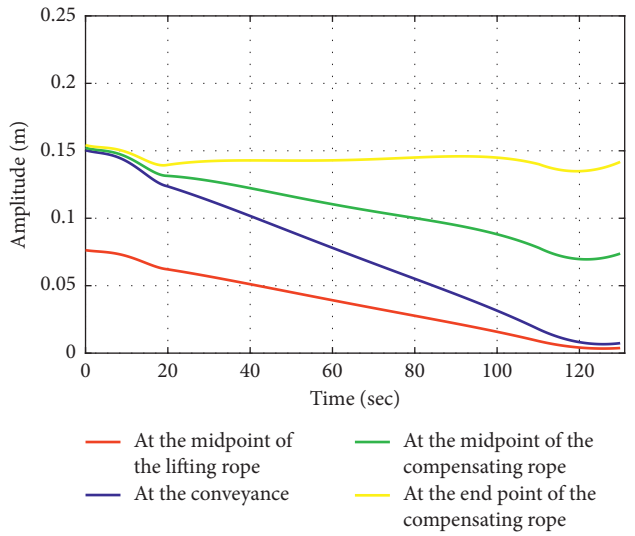

Figure 7: Longitudinal response trends of the traction system at different positions.

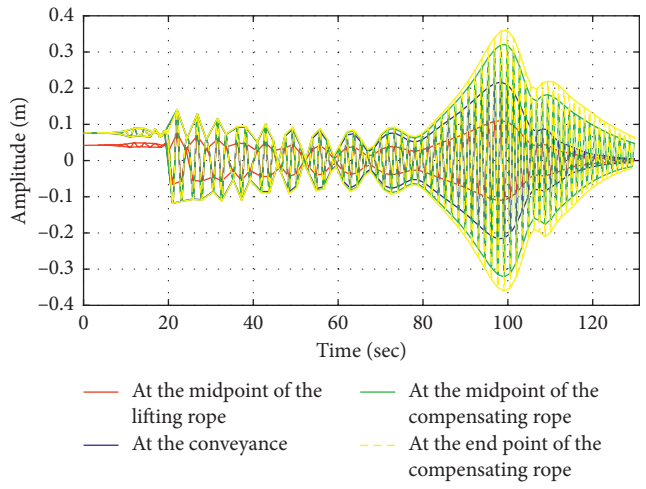

Figure 8: Longitudinal vibration of the traction system at different positions.

that the longitudinal vibration has transmissibility in a continuum from the top to bottom. In other words, the amplitude of longitudinal vibration increases gradually from the top to the end.

Figure 9 presents the longitudinal tensions of the traction system at different positions. The longitudinal tension at the connecting points of the lifting rope, compensating rope, and conveyance corresponds to plots (a), (b), and (c), respectively. In this figure, the black line represents the static tension caused by varying rope length and the mass of the conveyance. From these figures, the resonance region of the tension is exactly the same as that of the displacement, meaning they are positively correlated. In Figure 9, the amplitude of dynamical tension is much higher than that of static tension, especially in the resonance region.

3.2. Transverse Response. Figure 10 presents the transverse vibration responses at the midpoint of the lifting rope, midpoint of the compensating rope, and conveyance. By comparing these three observation points, one can see that the amplitude of transverse vibration at the midpoint of the

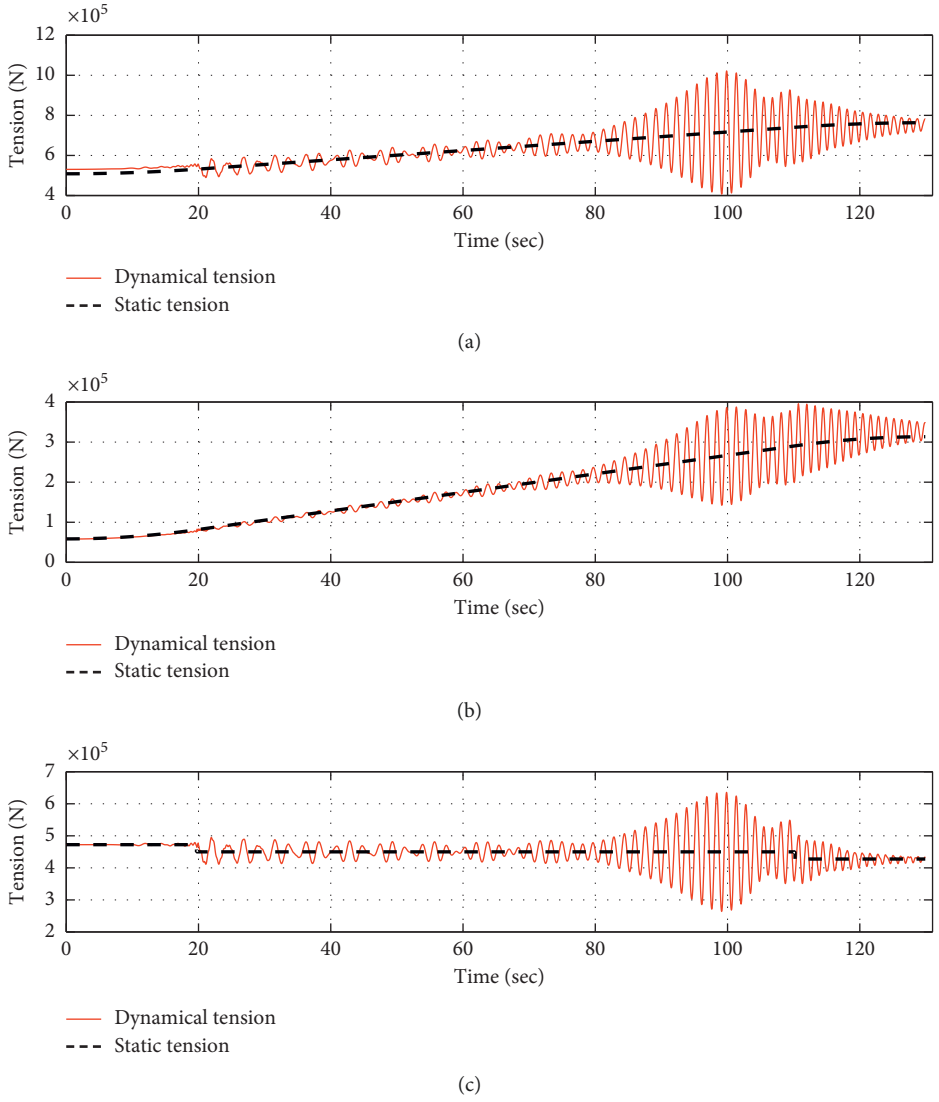

Figure 9: Longitudinal tension of the traction system at (a) connecting point A (shown in Figure 1), (b) connecting point B (shown in Figure 1), and the (c) conveyance.

lifting rope is much greater than that at the midpoint of the compensating rope. The point at which the transverse vibration amplitude is minimised is the conveyance.

In this system, excitation is transmitted from the drum to the conveyance and then to the compensating rope. Based on the constraints of the boundary conditions (guiding rope) at the conveyance, the amplitude of transverse vibrations at the conveyance is significantly reduced, meaning the excitation of the compensating rope is small. Therefore, the most violent transverse vibrations in the tensioned traction system occur at the midpoint of the lifting rope.

In Figure 10, one can see a resonance region. The resonance at the midpoint of the lifting rope begins at a time of 90 s and then decreases towards the end of the measured region. The maximum amplitude is 0.13 m, which significantly exceeds the excitation amplitude of 0.02 m.

Figure 11 presents the transverse vibrations at the connection points and conveyance. Although the observation points are all on the conveyance, the displacements of the transverse vibrations of these three observation points are inconsistent, especially in the final stages of lifting. This is because there are still small rotations at the conveyance caused by excitation and flexible guides, as shown in Figure 11(d). In the final stages of lifting, the angle of rotation of the conveyance increases to its maximum, which increases the inconsistency of transverse vibrations at the conveyance.

Figure 12 presents the transverse forces between the conveyance and ropes. Overall, the amplitude of the transverse forces gradually increases throughout the lifting cycle. After a time of 100 s, the frequency and amplitude of the transverse force increase significantly. From a horizontal comparison between connecting points A and B, one can see that the transverse forces at the connecting points are different, even though their transverse vibrations are similar. Through analysis and comparison, it can be concluded that the magnitudes of the transverse forces at the connection points are positively related to their individual rope tensions.

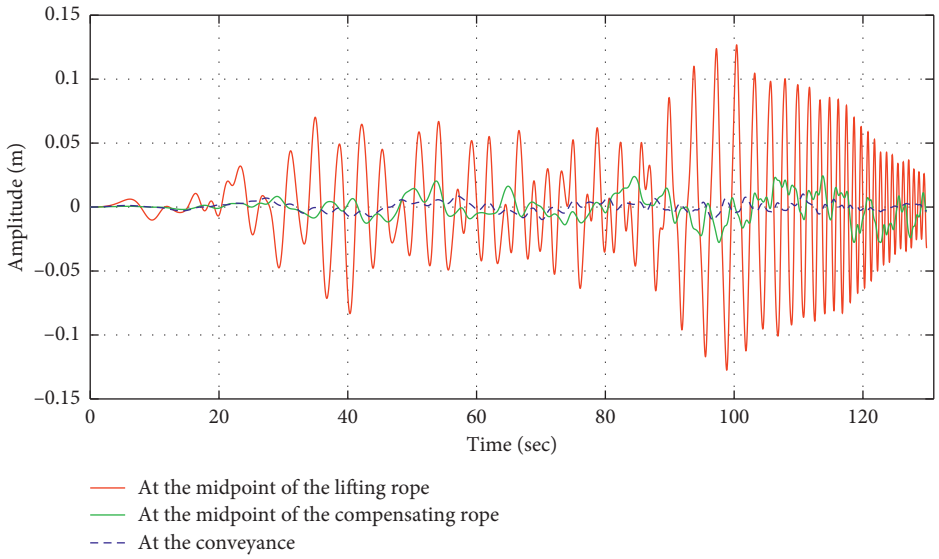

Figure 10: Transverse vibration responses at the midpoint of the lifting rope, midpoint of the compensating rope, and conveyance.

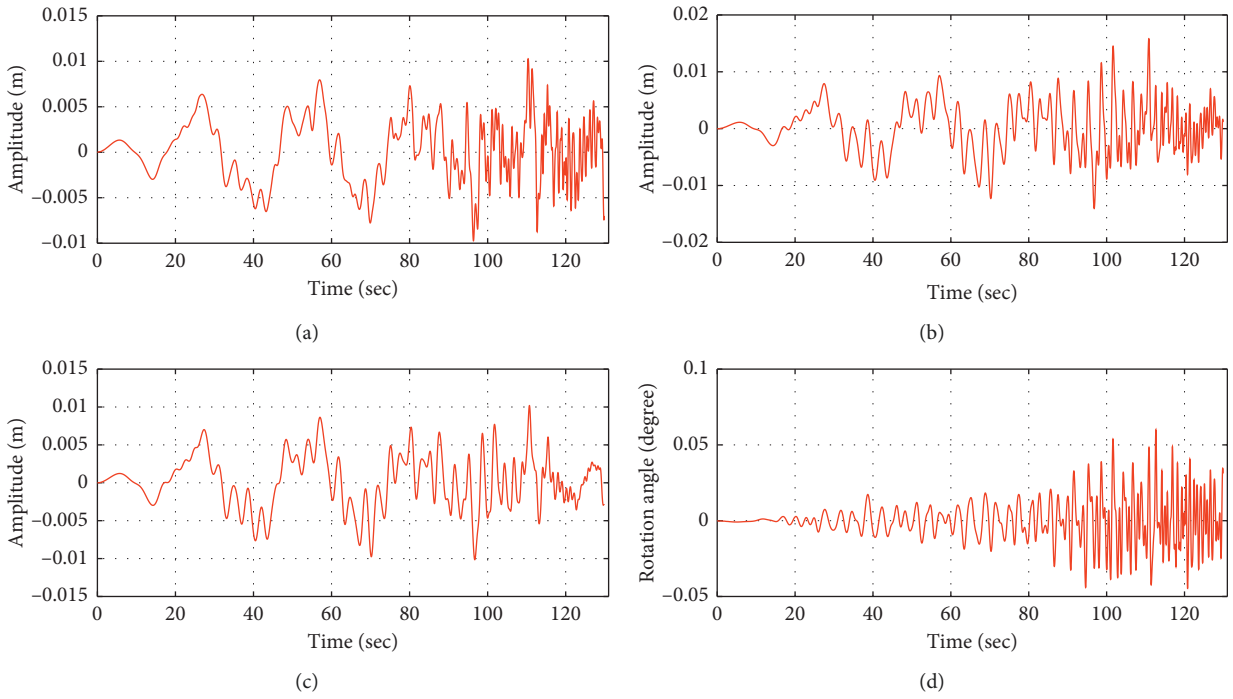

Figure 11: Transverse vibration at (a) connecting point A (shown in Figure 1), (b) connecting point B (shown in Figure 1), and the (c) conveyance. Plot (d) shows the rotation at the conveyance.

4. Comparison between Traditional Traction System and Tensioned Traction System

Previous studies have largely focused on traditional traction systems. In previous studies, many scholars have considered the compensating rope as a time-varying concentrated mass located inside the conveyance. Wu et al. [24] established a transverse vibration model using the Hamilton principle, which considers ropes as continuums, and obtained the transverse vibration characteristics of a traditional traction system. Traction systems with terminal tension acting on the compensating rope represent a novel type of lifting system. To analyse the differences between this new type of system and a traditional traction system, the mathematical model from [25] is considered in this paper. A physical model and equivalent mathematical model of a traditional traction system are presented in Figure 13.

As shown in Figure 13, in a traditional traction system, the compensation rope is in a free suspension state. In this situation, the compensating rope can be considered as blocks of variable mass at the end of the conveyance, which are denoted as m_e. The mass of the blocks is equal to the product

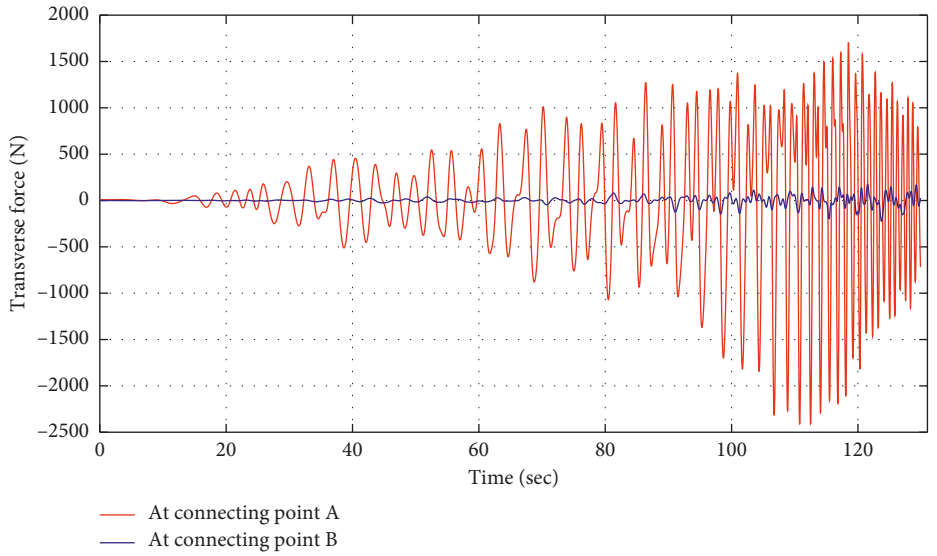

Figure 12: Transverse forces between the conveyance and ropes.

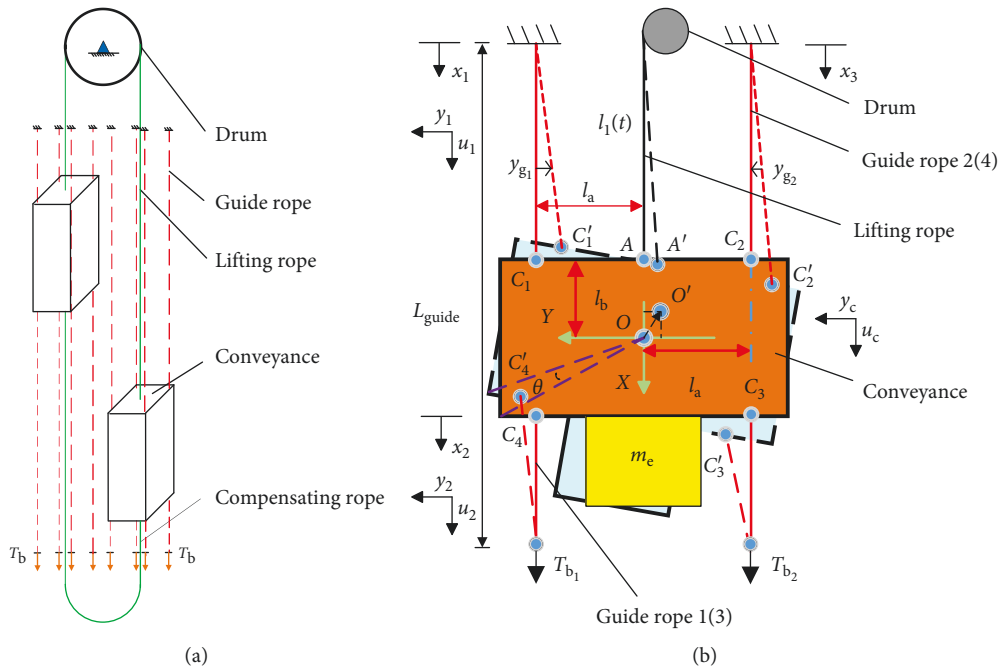

Figure 13: (a) Physical model and (b) mathematical model of a traditional traction system.

of line density and the length of the compensating rope. Therefore, this value varies with time. The Lagrange equation was used to establish the mathematical model. The dynamic characteristics of the traditional traction system model can be obtained using numerical solution methods.

4.1. Longitudinal Response Comparison between Traditional Traction System and Traction System with Terminal Tension. Based on the referenced model, the dynamical responses of a traditional traction system can be obtained using numerical solution methods. Figure 14 presents a comparison of the longitudinal responses at the conveyance between a traction system with terminal tension and a traditional traction system.

It is clear that the longitudinal vibration at the conveyance with terminal tension is smaller than that in the traditional traction system. From the beginning of lifting to a time of 60 s, the vibration displacements at the conveyances of the two systems are nearly the same. However, the amplitude of the traction system with terminal tension acting on the compensating rope is much smaller than that of the traditional traction system when the systems operate inside the resonance zone. Overall, from a time of 80 s to the end of lifting, the terminal tension on the compensating rope can significantly restrain the longitudinal vibration of the

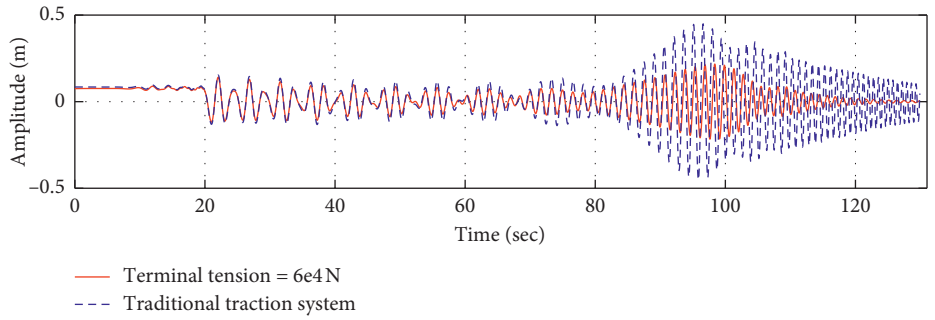

Figure 14: Comparison of the longitudinal vibrations at the conveyance between a traction system with a terminal tension of 6×10^4 N (red line) and a traditional traction system (blue line).

conveyance. Changes in the physical properties of the compensating rope result in a change in the amplitude of the longitudinal vibrations. Here, the compensating rope is considered as a spring with time-varying stiffness and mass. The tensioned compensating rope acts as a shock absorber. In a traditional traction system, the compensating rope is not tightened and does not have the nature of a spring.

In Figure 14, it is clear that the resonance regions of the traditional traction system and the traction system with terminal tension are different. Figure 15 verifies this finding. In this figure, one can see that the locations of the intersection points between the excitation frequency and first natural frequency of the two-traction systems are different. Consider the first-order natural frequencies in Figure 15 as an example. One can see that the first-order natural frequencies of the two-traction system are significantly different when the position of the conveyance is between the initial position and 400 m. The frequency of the traditional traction system is much greater than that of the tensioned traction system. However, when the position of the conveyance exceeds 400 m, the frequencies of the two systems are nearly identical. Therefore, it can be concluded that the change in longitudinal natural frequency is greater for the traction system with a tensioned compensating rope only when the compensation rope is long. This finding also applies to higher orders of natural frequencies.

4.2. Transverse Response Comparison between Traditional Traction System and Traction System with Terminal Tension. Figures 16–18 present comparisons of the natural frequencies of transverse vibrations of the traditional traction system and tensioned traction system.

Regarding the natural frequencies in Figure 18, the frequency of the traditional traction system is greater than that of the tensioned traction system in most stages for corresponding orders. However, there is always an intersection of corresponding orders and the frequency of the tensioned traction system will ultimately exceed that of the traditional traction system. To analyse dynamical responses, the midpoint of the lifting rope and conveyance were selected as two observation points. From Figures 16 and 17, one can see that the trends of the transverse vibrations of both traction systems are similar. In other words, it can be concluded that the tension on the compensating rope has little effect on the transverse vibration of a system.

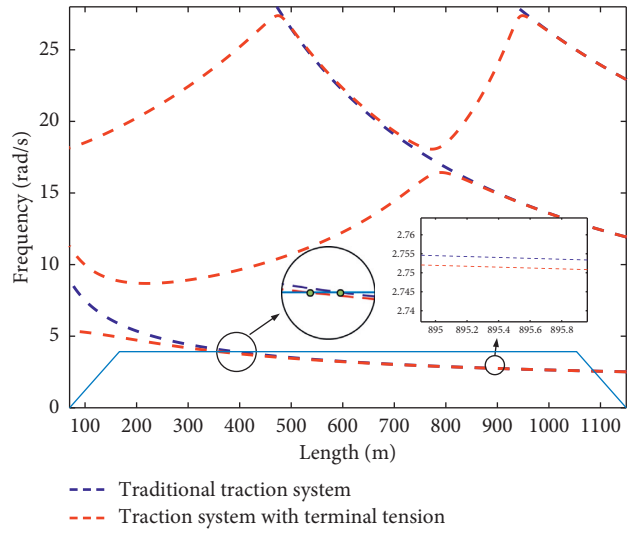

Figure 15: Comparison of the natural frequencies of the two-traction systems.

5. Response Comparisons of Tensioned Traction Systems with Different Terminal Tensions

5.1. Longitudinal Response Comparisons with Different Terminal Tensions. Applying different tensions to the compensating rope will produce different dynamic responses. Therefore, it is necessary to analyse the dynamic responses of the tensioned traction system under different terminal tensions. Figure 19 presents the longitudinal vibration frequencies of the traction system with different tensions acting on the compensating rope. The red line represents for the longitudinal natural frequency of the traction system. The blue line represents the frequency of longitudinal excitation. The green point represents the intersection between the natural frequency and frequency of excitation.

In Figure 19, three different terminal tensions (tension $= 4 \times 10^4$ N, 6×10^4 N, and 8×10^4 N) on the compensating rope are presented for comparison. One

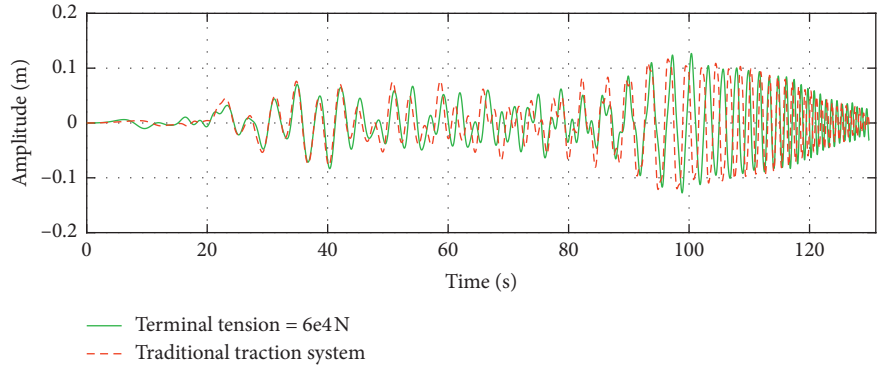

Figure 16: Comparison of transverse vibration displacements of the lifting ropes at the midpoint.

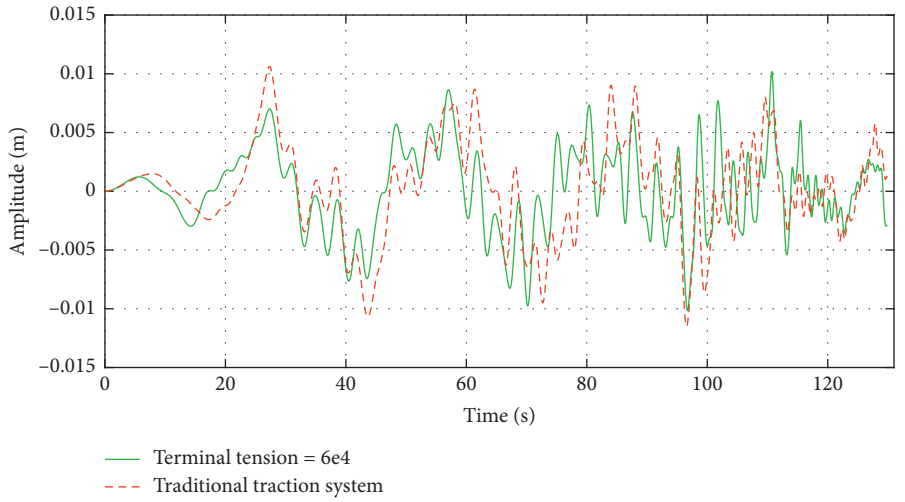

Figure 17: Comparison of transverse vibration displacements at the conveyance.

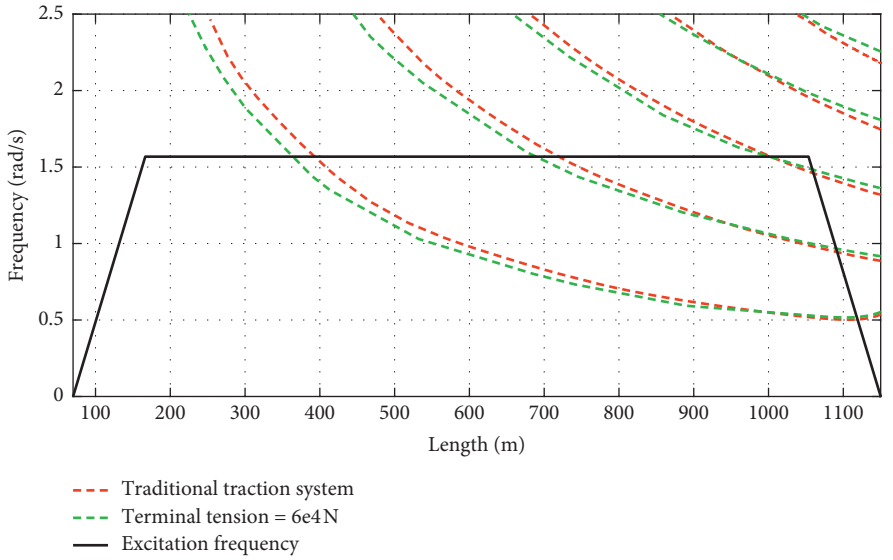

Figure 18: Comparison of natural frequencies of transverse vibrations.

can see that the longitudinal natural frequency of the system does not change with different tensions acting on the compensating rope. Therefore, the position of the intersection does not change. It can be concluded that the longitudinal natural frequency is independent of the terminal tension.

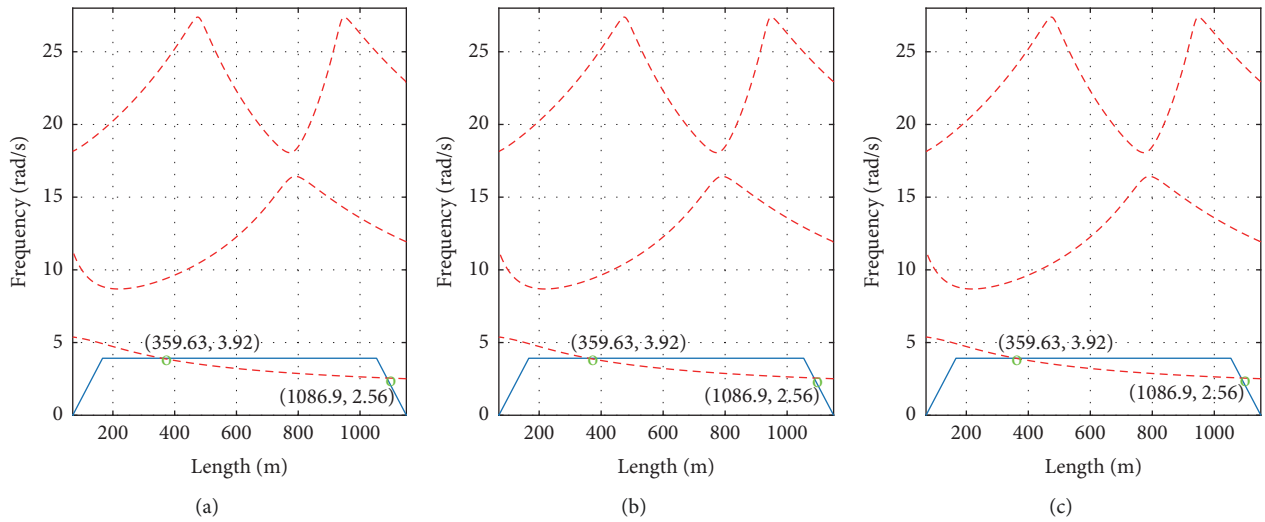

Figure 19: Longitudinal vibration frequencies of the traction system. (a) Tension = 4×10^4 N, (b) tension = 6×10^4 N, and (c) tension = 8×10^4 N.

Figure 20 presents the longitudinal responses of the tensioned traction system with different terminal tensions. To obtain vibration characteristics, the longitudinal vibrations were divided into two parts: vibration displacement and elastic elongation. The conveyance was selected as the observation point. The results are presented in Figures 21 and 22.

In Figure 21, by comparing the longitudinal vibrations at different terminal tensions, one can see that the shapes of the longitudinal vibrations with different terminal tensions acting on the compensating rope do not change. However, the negative slope of the trend of longitudinal vibration becomes gradually steeper with an increase in tension acting on the compensating rope. Therefore, the elastic elongation of the rope is proportional to the terminal tension. In summary, the shapes of vibration and natural frequency curves do not change with the terminal tension acting on the compensating rope, but elastic elongation does change.

5.2. Transverse Response Comparisons between Traction Systems with Different Terminal Tensions. The main reason for the resonance in transverse vibrations is the intersection between the excitation frequency and natural frequency of the system. Therefore, it is necessary to analyse natural frequency changes according to the terminal tension acting on the compensating rope. The variations in frequency corresponding to all transverse modes of the ropes with a terminal tension of 5×10^4 N acting on the compensating rope are presented in Figure 23.

In Figure 23, the red, green, and yellow lines represent the natural frequencies of the compensating, lifting, and guiding ropes, respectively. The blue line represents the frequency of excitation. Overall, one can see that the natural frequency of the lifting rope decreases as the length of the lifting rope increases. In contrast, the natural frequency of the compensating rope increases. One can see that the natural frequencies of the lifting rope are much higher than those of the compensating rope for each corresponding order when they are measured on the corresponding length scales. This is mainly caused by the difference in tension between these ropes. The tension on the lifting rope consists of not only its own gravity but also the gravity of the conveyance and compensating rope, and the terminal tension acting on the compensating rope. Regarding the compensating rope, its tension only consists of its own gravity and the terminal tension. These differences in tension result in differences in stiffness, which affect the natural frequencies of ropes. Therefore, in Figure 23, the lifting rope shows a much higher frequency than the compensating rope in the same coordinate dimension.

The natural frequencies of the traction system can be divided into three parts, namely, the frequencies of the guiding, lifting, and compensating ropes. The variations in the frequencies of the lifting and compensating ropes with different terminal tensions are presented in Figure 24.

The variation in the natural frequency of the lifting rope is presented in Figure 24(a), while that of compensating rope is shown in Figure 24(b). In Figure 24, the red, green, and blue lines represent the variations in the natural frequencies of the lifting and compensating ropes with terminal tensions of 2×10^4 N, 5×10^4 N, and 1×10^5 N acting on the compensating rope, respectively. It is evident that the transverse frequencies of the lifting and compensating ropes increase as the tension acting on the compensating rope increases. The increase in natural frequency is proportional to the terminal tension. By comparing Figures 24(a) and 24(b), one can see that the increase in the amplitude of the natural frequency of the lifting rope is much smaller than that of the compensating rope with the same increase in terminal tension. Therefore, the natural frequencies of the compensating rope are more sensitive to variation in terminal tension than those of the lifting rope. Logically, the resonance region of the midpoint of the lifting rope will also change accordingly although the

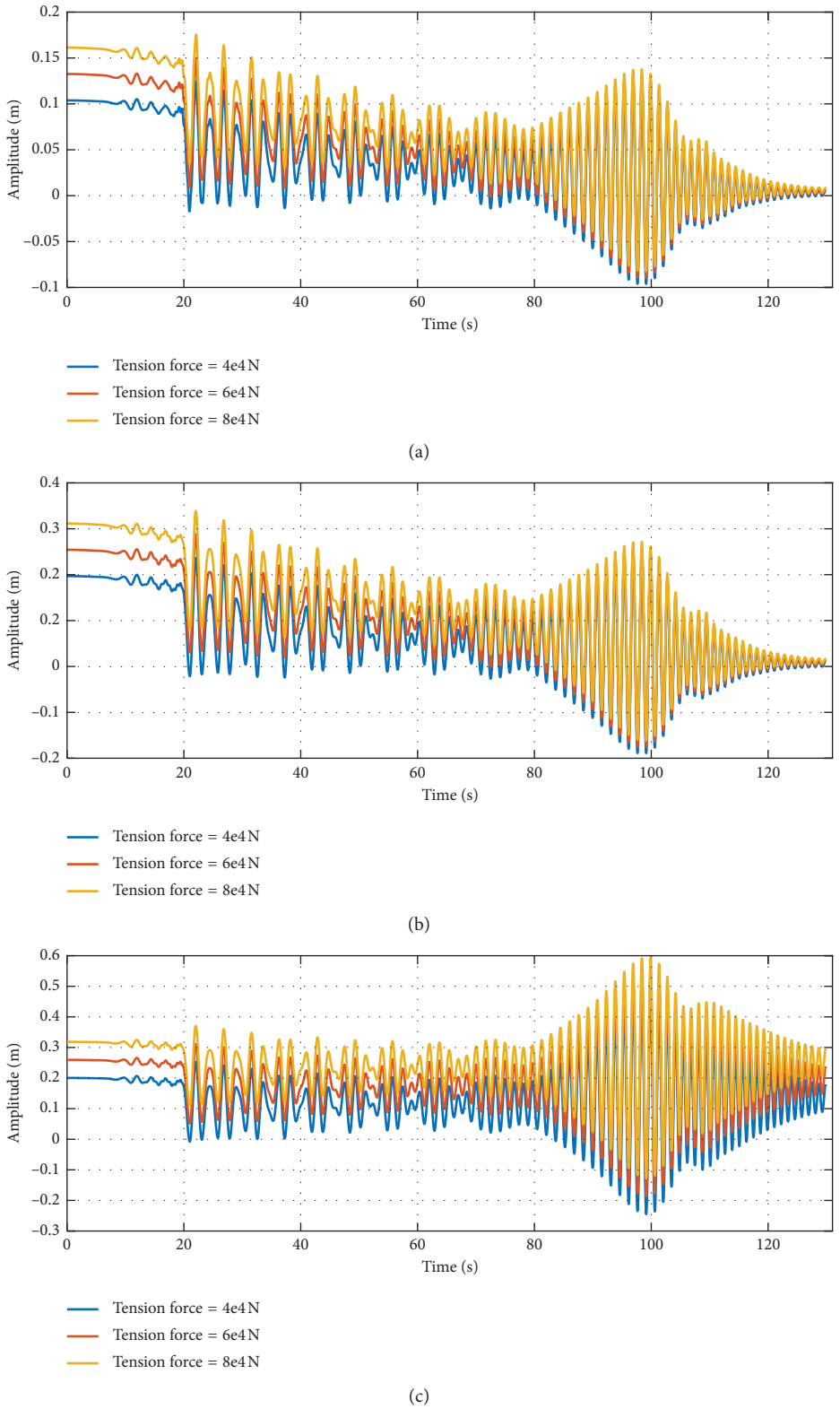

Figure 20: Longitudinal responses of the tensioned traction system at the (a) midpoint of the lifting rope, (b) conveyance, and (c) end point of the compensating rope.

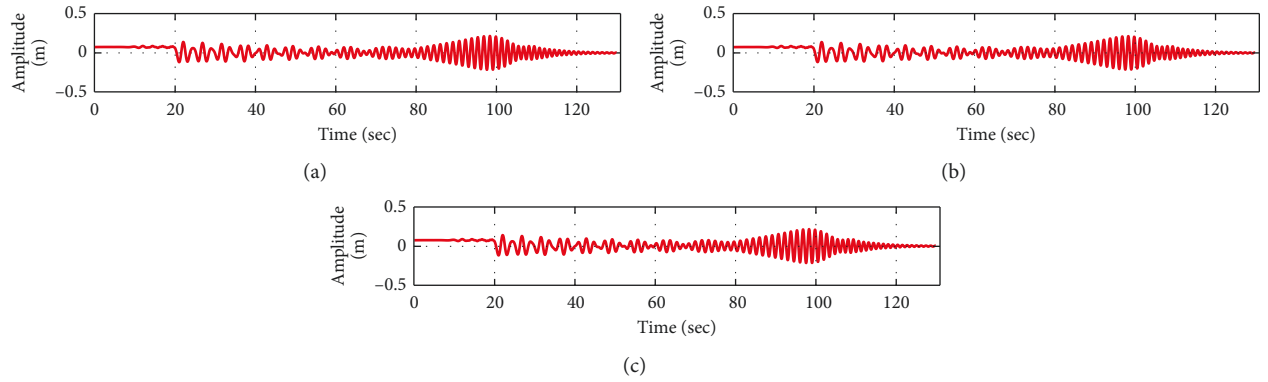

Figure 21: Longitudinal vibration displacements of the tensioned traction system. (a) Terminal tension = 4×10^4 N, (b) terminal tension = 6×10^4 N, and (c) terminal tension = 8×10^4 N.

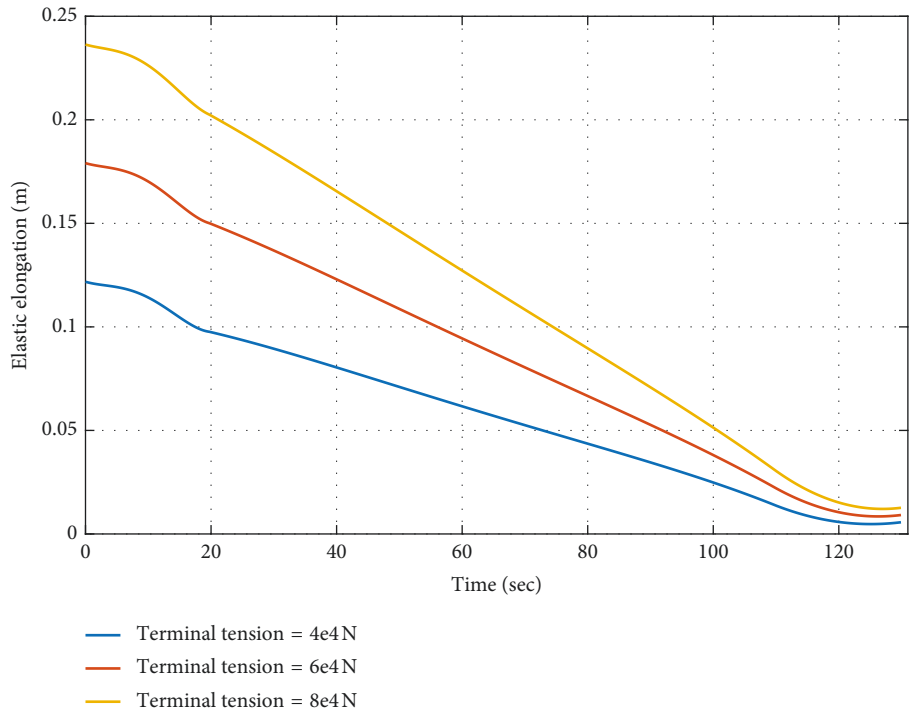

Figure 22: Elastic elongation displacements of the tensioned traction system. (a) Terminal tension = 4×10^4 N, (b) terminal tension = 6×10^4 N, and (c) terminal tension = 8×10^4 N.

magnitude of the change is relatively small. This variation in the resonance region is presented in Figure 25. Regarding the compensating rope, its transverse vibration characteristics do not change significantly when applying different terminal tensions, so they are not discussed further.

6. Dynamical Behaviour of the Guiding Rope

6.1. Dynamical Responses. When tension is applied to the end of the compensating rope, the properties of the system change and affect the dynamic characteristics of the guiding rope. Therefore, it is necessary to analyse the differences in the dynamical responses of the guiding rope in a tensioned system and traditional system.

Through numerical simulations, the transverse displacements of the guiding rope were obtained. The results are presented in Figure 26. The transverse displacements of the two guide ropes are identical based on consistent preloading. Therefore, only one rope is represented for the time period of 10 s to 110 s in Figure 26. In this figure, the "*" marker represent the upper and lower boundaries of the conveyance, which can characterise the lifting position and rotation of the conveyance (Figure 27).

In Figure 26, the amplitude and vibration frequency of the guiding rope increase as the conveyance is lifted up. At a time of 110 s, high-order modes of the guiding rope are considered, meaning the results can represent all vibrations of the guiding rope. By comparing Figures 26 and 11(d), it can be concluded that the increase in the amplitude and

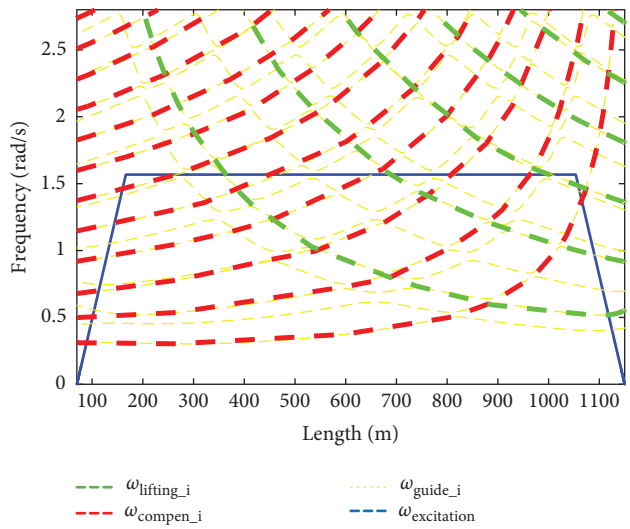

Figure 23: Natural frequencies of the lifting, compensating, and guiding ropes.

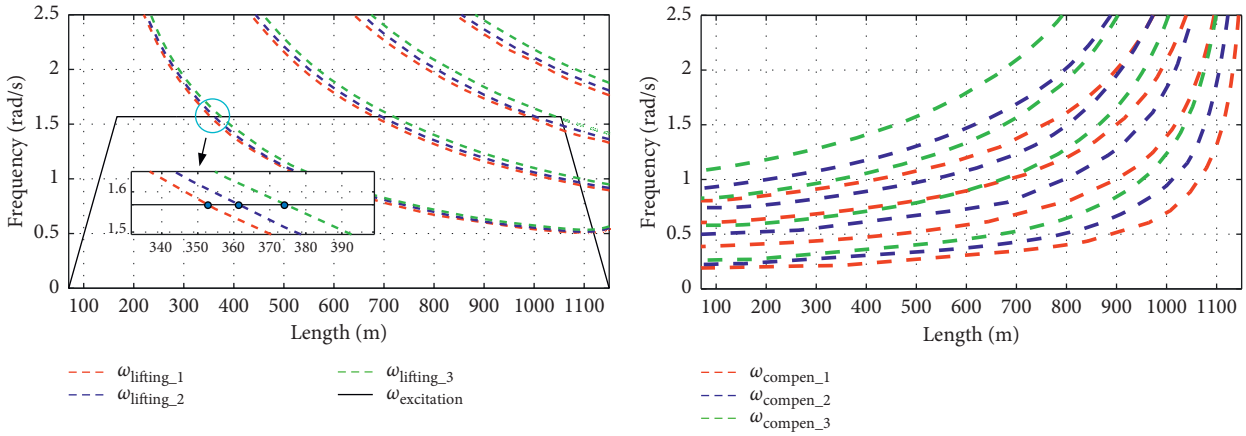

Figure 24: Variations in the transverse natural frequencies of the lifting and compensating rope, where $\omega_{lifting-1,2,3}$ is the transverse natural frequency of the lifting rope, $\omega_{compen-1,2,3}$ is the transverse natural frequency of the compensating rope, and $\omega_{excitation}$ is the excitation frequency in the transverse direction.

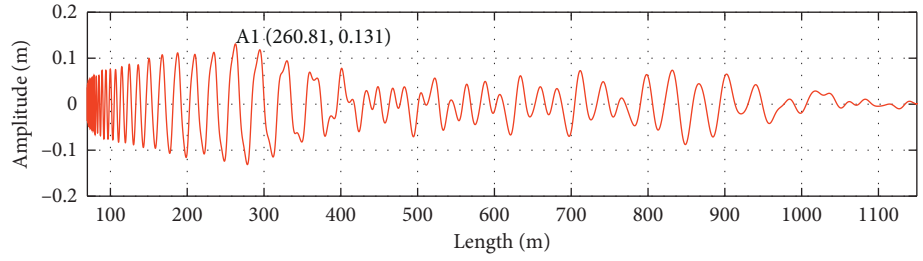

Figure 25: Continued.

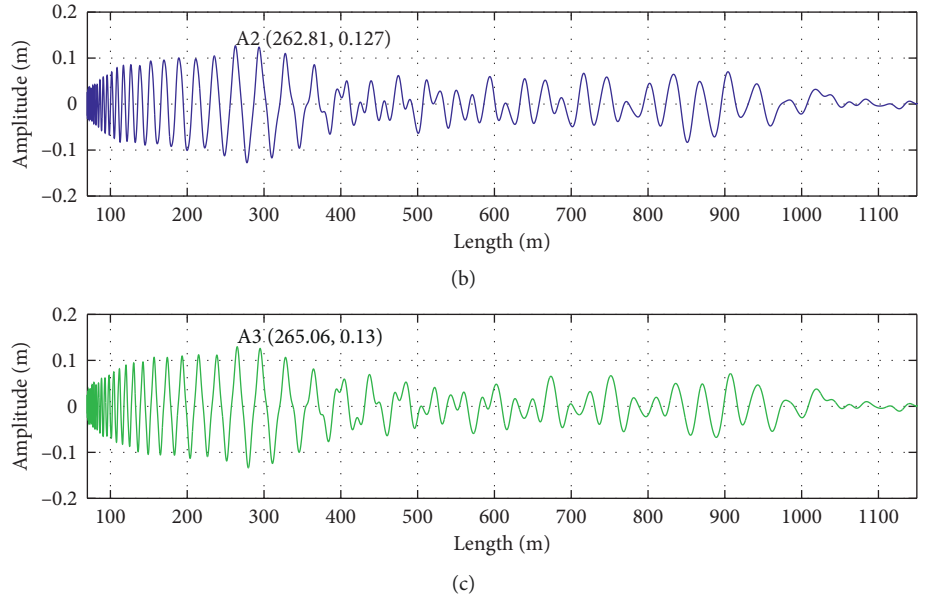

Figure 25: Variation in the resonance region at the midpoint of the lifting rope. (a) Terminal tension = 2×10^4 N, (b) terminal tension = 5×10^4 N, and (c) terminal tension = 1×10^5 N.

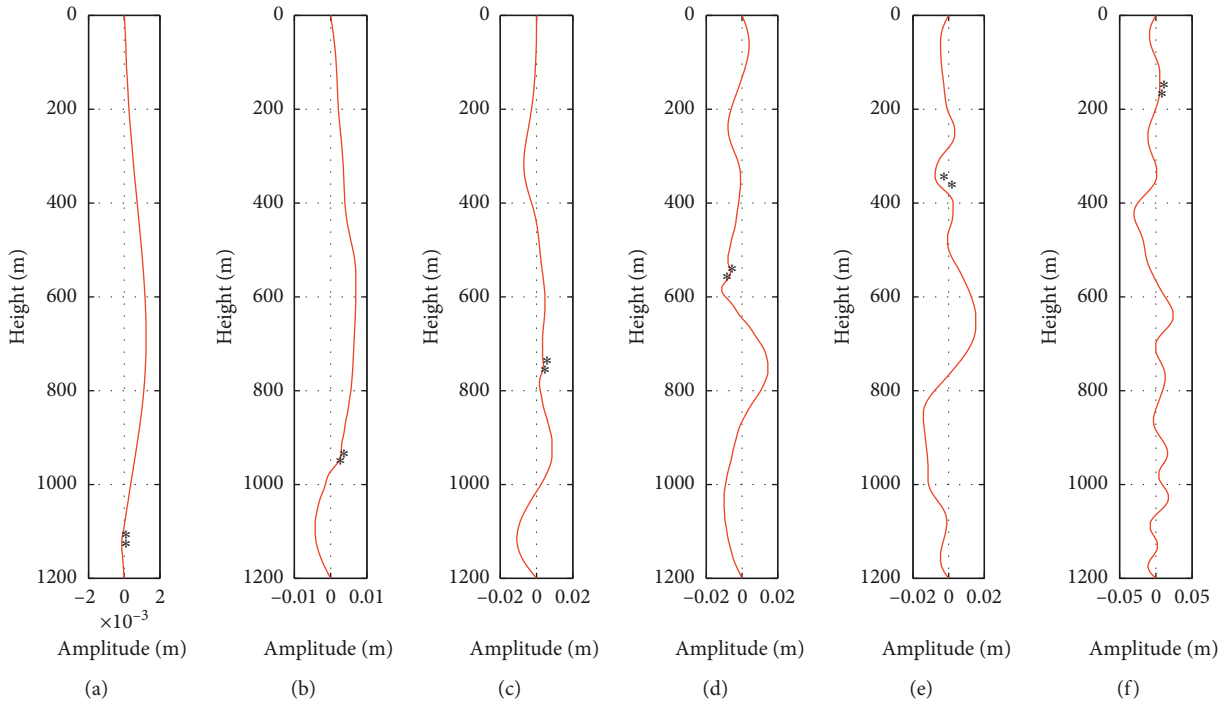

Figure 26: Transverse displacement of the guiding rope of the traction system at different times.

frequency of transverse vibration at the end of guiding rope is caused by the influence of transverse vibration at the conveyance. In other words, the vibration of the conveyance is the source of excitation for the guiding rope.

The transverse connecting force between the conveyance and guiding ropes can be observed in Figures 27 and 28. As shown in Figure 28, C_1 and C_4 are the connection points between the left guiding rope and conveyance and are located at the upper and lower boundaries of the conveyance, respectively. Because the height of the conveyance is small when compared to the length of the guiding rope, the trends in the transverse vibrations and connecting forces of connecting points C_1 and C_4 are generally consistent with a few small differences. The main reason for these differences is the rotation of the conveyance. The amplitude of the transverse vibrations at connecting point C_4 is larger than that at C_1.

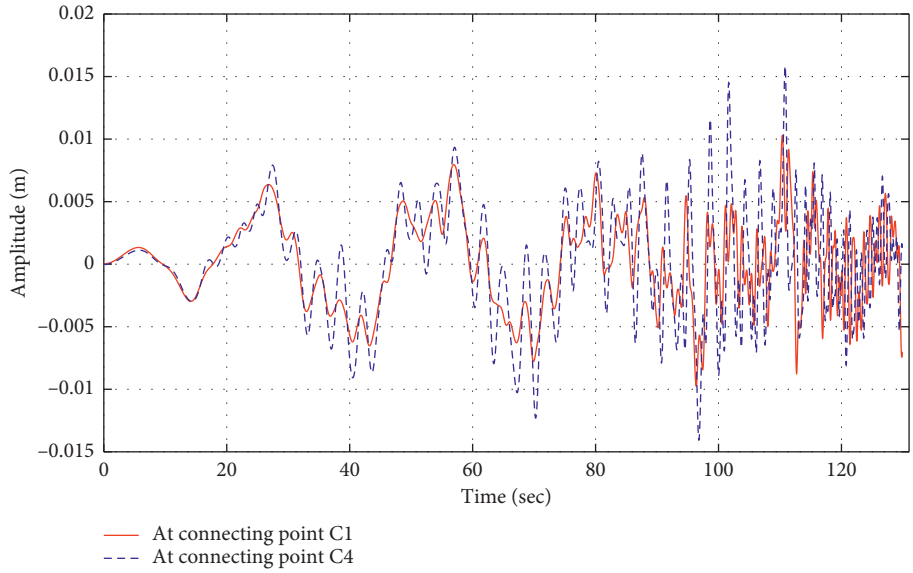

Figure 27: Comparison of the transverse vibrations of the traction system at the connecting points.

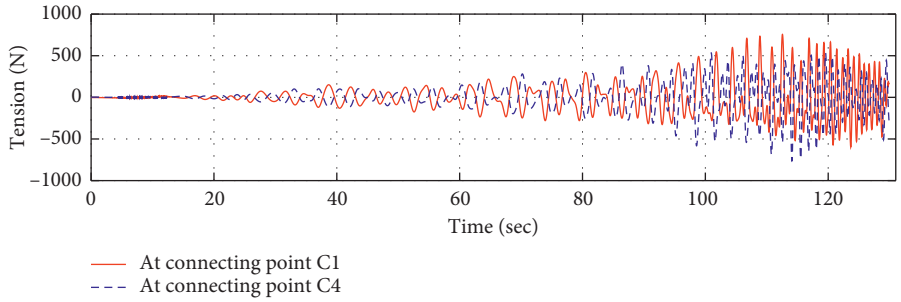

Figure 28: Comparison of the transverse force of the traction system at the connecting points.

6.2. Comparisons. Figure 29 presents a comparison of the transverse vibration displacements of the connecting points in a tensioned traction system and traditional traction system.

In Figures 29 and 30, one can see that the transverse amplitude of the tensioned traction system is smaller than that of the traditional traction system in most stages. However, in some stages, the terminal tension cannot act as a significant restraint. For example, in Figure 30(b), the amplitude of the tensioned traction system is greater than that of the traditional traction system at times of approximately 80 s and 100 s. In Figure 30, one can see that the transverse connecting force of the tensioned traction system is much smaller than that of the traditional traction system in most stages. Overall, terminal tension can reduce the transverse vibrations of the connection point between the guiding rope and conveyance, but it cannot play a significant role in some local areas. By applying tension at the end of the compensating rope, the transverse connecting force between the guiding ropes and conveyance is reduced.

7. Conclusion

In this paper, the dynamical behaviour of a traction system with terminal tension acting on the compensating rope was investigated. A model for the tensioned traction system was established using an energy-based method. A dynamical equation was derived using the first-order Lagrange equation. The longitudinal and transverse dynamic behaviours of the lifting, compensating, and guiding ropes were modelled. The ropes were spatially discretised using the AMM, and results were obtained using numerical methods. First, the longitudinal and transverse responses of the tensioned traction system were analysed in detail. Second, we compared the analysis results to those of a traditional traction system and determined that terminal tension acting on the compensating rope can restrain the longitudinal vibration of the conveyance, including in the resonance region. However, tension has no significant effect on the suppression of transverse vibrations in the system. It was shown that the longitudinal vibrations of the lifting and compensating ropes do not change significantly with different levels of terminal tension on the compensating rope, which can only affect the elastic elongation of the ropes. The system's natural frequencies of transverse vibration were calculated accurately. Through comparisons, it was determined that the natural frequencies of the compensating rope are more sensitive to variations in terminal tension than those of the lifting rope. Finally, the shape and vibration responses of the guiding rope were simulated accurately.

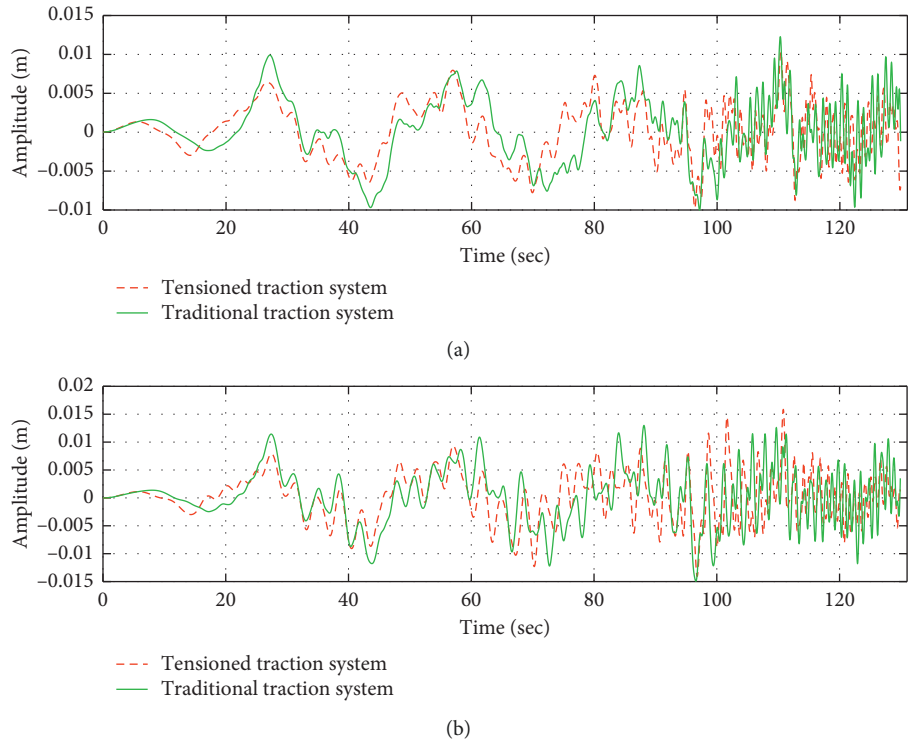

Figure 29: Comparison of the transverse vibration displacements of the connecting points in a tensioned traction system and traditional traction system; (a) connecting point C_1; (b) connecting point C_2.

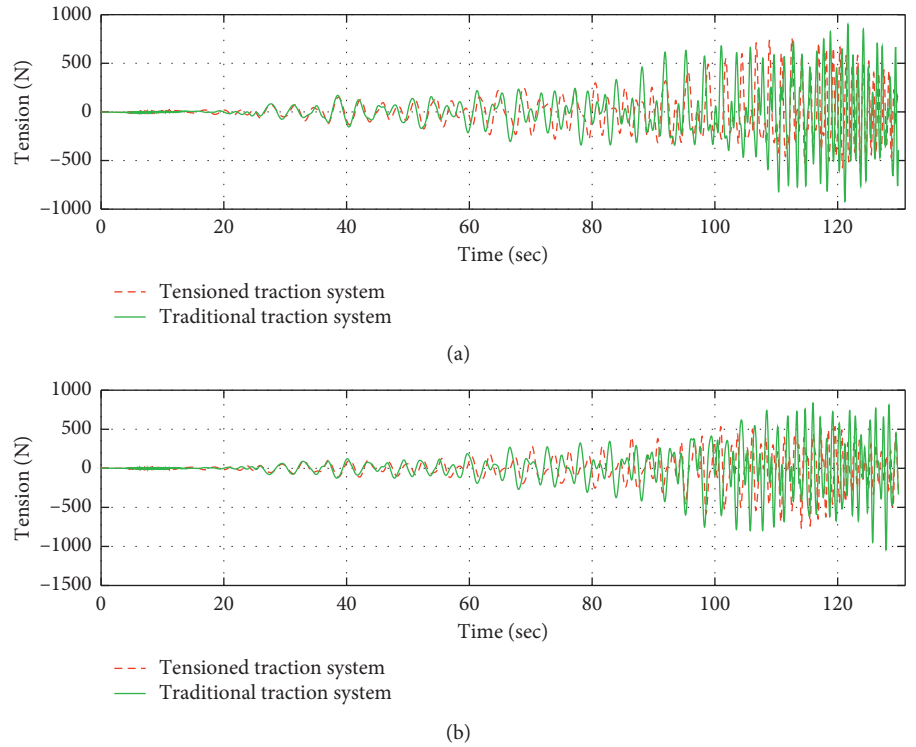

Figure 30: Comparison of the transverse connecting forces in a tensioned traction system and traditional traction system; (a) connecting point C_1; (b) connecting point C_2.

Compared to a traditional traction system, a traction system with terminal tension can suppress the transverse vibrations and transverse forces of the connecting points between the guiding ropes and the conveyance to a certain degree.

Based on the analysis above, the dynamical characteristics and inherent properties of a tensioned traction system were detailed. Differences compared to a traditional traction system were also discussed in detail, meaning these results should serve as a helpful guide for the design and optimisation of traction systems.

Appendix

A. Tensions of the Ropes

The tensions at arbitrary positions along the lifting, compensating, and guiding ropes are calculated as follows:

$$T_1(x_1,t) = [m_c g + \rho_1 (l_1(t) - x_1)](g - a_1), \quad 0 \le x_1 \le l_1(t), \tag{A.1}$$

$$T_2(x_2,t) = [m_c g + \rho_2 (l_2(t) - x_2)](g - a_2), \quad 0 \le x_2 \le l_2(t), \tag{A.2}$$

$$\begin{aligned} T_{g_1}(x_3,t) &= T_{b_1} + \rho_g g\left(L_{\text{guide}} - x_3\right), \\ T_{g_2}(x_3,t) &= T_{b_2} + \rho_g g\left(L_{\text{guide}} - x_3\right), \\ &0 \le x_3 \le L_{\text{guide}}. \end{aligned} \tag{A.3}$$

B. Constraint Conditions

The constraint conditions for the rope-guided traction system are defined as follows:

$$g_1(t) = \begin{bmatrix} u_1(l(t),t) = u_c + l_b(1 - \cos\theta) \\ y_1(l(t),t) = y_c - l_b \sin\theta \end{bmatrix}, \tag{B.1}$$

$$g_2(t) = \begin{bmatrix} u_2(0,t) = u_c + l_b(\cos\theta - 1) \\ y_2(0,t) = y_c + l_b \sin\theta \end{bmatrix}, \tag{B.2}$$

$$g_3(t) = \begin{bmatrix} y_{C_1}(l(t),t) = y_c - l_b \sin\theta + l_a(\cos\theta - 1) \\ y_{C_2}(l(t),t) = y_c + l_a(1 - \cos\theta) - l_b \sin\theta \\ y_{C_3}(l(t) + 2l_b,t) = y_c + l_b \sin\theta + l_a(1 - \cos\theta) \\ y_{C_4}(l(t) + 2l_b,t) = y_c + l_b \sin\theta + l_a(\cos\theta - 1) \end{bmatrix}. \tag{B.3}$$

When $\sin\theta \approx \theta$, $\cos\theta \approx 1$, the constraint conditions can be simplified as follows:

$$g_1(t) = \begin{bmatrix} u_1(l(t),t) = u_c \\ y_1(l(t),t) = y_c - l_b\theta \end{bmatrix}, \tag{B.4}$$

$$g_2(t) = \begin{bmatrix} u_2(0,t) = u_c \\ y_2(0,t) = y_c + l_b\theta \end{bmatrix}, \tag{B.5}$$

$$g_3(t) = \begin{bmatrix} y_{C_1}(l(t),t) = y_c - l_b\theta \\ y_{C_2}(l(t),t) = y_c - l_b\theta \\ y_{C_3}(l(t) + 2l_b,t) = y_c + l_b\theta \\ y_{C_4}(l(t) + 2l_b,t) = y_c + l_b\theta \end{bmatrix}. \tag{B.6}$$

C. Elements of Matrix of Dynamics Equation

The matrices and force vectors for the tensioned traction system are defined in the following forms:

$$\begin{aligned} M(t) &= \text{diag}\left(M_{y_1}(t), M_{y_2}(t), M_{u_1}(t), M_{u_2}(t), M_{y_{g_1}}(t), M_{y_{g_2}}(t), M_c, M_c, J_c\right), \\ C(t) &= \text{diag}\left(C_{y_1}(t), C_{y_2}(t), C_{u_1}(t), C_{u_2}(t), C_{y_{g_1}}(t), C_{y_{g_2}}(t), 0, 0, 0\right), \\ F(t) &= \left[F_{y_1}(t); F_{y_2}(t); F_{u_1}(t); F_{u_2}(t); F_{y_{g_1}}(t); F_{y_{g_2}}(t); F_c; 0; 0\right], \\ N(t) &= \left[N_{y_1}(t); N_{y_2}(t); N_{u_1}(t); N_{u_2}(t); 0; 0; 0; 0; 0\right], \\ K(t) &= \begin{bmatrix} K_{y_1}(t) & 0 & K_{u_1-y_1}(t) & 0 & 0 & 0 & 0\ 0\ 0 \\ 0 & K_{y_2}(t) & 0 & K_{u_2-y_2}(t) & 0 & 0 & 0\ 0\ 0 \\ K_{y_1-u_1}(t) & 0 & K_{u_1}(t) & 0 & 0 & 0 & 0\ 0\ 0 \\ 0 & K_{y_2-u_2}(t) & 0 & K_{u_2}(t) & 0 & 0 & 0\ 0\ 0 \\ 0 & 0 & 0 & 0 & K_{y_{g_1}}(t) & 0 & 0\ 0\ 0 \\ 0 & 0 & 0 & 0 & 0 & K_{y_{g_2}}(t) & 0\ 0\ 0 \\ 0 & 0 & 0 & 0 & 0 & 0 & 0\ 0\ 0 \\ 0 & 0 & 0 & 0 & 0 & 0 & 0\ 0\ 0 \\ 0 & 0 & 0 & 0 & 0 & 0 & 0\ 0\ 0 \end{bmatrix}. \end{aligned} \tag{C.1}$$

The specific forms of the elements in matrices $M_{u_k}, M_{y_k}, C_{u_k}, C_{y_k}, K_{u_k}, K_{y_k}, F_{u_k}, F_{y_k}, F_{u_c}$, and F_{y_c} are defined as follows:

$$\begin{aligned} M_{u_k,ji} &= \rho_k l_k(t) \int_0^1 \left(\sum_{i=1}^{N} \phi_{ki}\phi_{kj} \right) d\xi, \\ M_{y_k,ji} &= \rho_k l_k(t) \int_0^1 \left(\sum_{i=1}^{N} \kappa_{ki}\kappa_{kj} \right) d\xi, \end{aligned} \tag{C.2}$$

$$\begin{aligned} C_{u_k,ji} &= \rho_k v_k \int_0^1 (1-\xi) \sum_{i=1}^{N} \phi'_{ki}\phi_{kj} d\xi + \rho_k v_k \int_0^1 \sum_{i=1}^{N} \phi_{ki}\phi_{kj} d\xi \\ &\quad - \rho_k v_k \int_0^1 (1-\xi) \sum_{i=1}^{N} \phi_{ki}\phi'_{ki} d\xi \\ &\quad + \mu_k \rho_k l_k(t) \int_0^1 \left(\sum_{i=1}^{N} \phi_{ki}\phi_{kj} \right) d\xi, \\ C_{y_k,ji} &= \rho_k v_k \int_0^1 (1-\xi) \sum_{i=1}^{N} \kappa'_{ki}\kappa_{kj} d\xi + \rho_k v_k \int_0^1 \sum_{i=1}^{N} \kappa_{ki}\kappa_{kj} d\xi \\ &\quad - \rho_k v_k \int_0^1 (1-\xi) \sum_{i=1}^{N} \kappa_{ki}\kappa'_{ki} d\xi \\ &\quad + \zeta_k \rho_k l_k(t) \int_0^1 \left(\sum_{i=1}^{N} \kappa_{ki}\kappa_{kj} \right) d\xi, \end{aligned} \tag{C.3}$$

$$\begin{aligned} K_{u_k,ji} &= \rho_k a_k \int_0^1 (1-\xi) \sum_{i=1}^{N} \phi'_{ki}\phi_{kj} d\xi + \frac{\rho_k v_k^2}{l_k} \int_0^1 \xi \sum_{i=1}^{N} \phi'_{ki}\phi_{kj} d\xi \\ &\quad - \frac{\rho_k v_k^2}{l_k} \int_0^1 \left((1-\xi)^2 \sum_{i=1}^{N} \phi'_{ki}\phi'_{ki} \right) d\xi \\ &\quad + \frac{EA}{l_k} \int_0^1 \sum_{i=1}^{N} \phi'_{ki}\phi'_{ki} d\xi \\ &\quad - \mu_k \rho_k v_k \int_0^1 \left(\xi \sum_{i=1}^{N} \phi'_{ki}\phi_{kj} \right) q_{ki}(t) d\xi, \\ K_{y_k,ji} &= \rho_k a_k \int_0^1 (1-\xi) \sum_{i=1}^{N} \kappa'_{ki}\kappa_{kj} d\xi \\ &\quad + \frac{\rho_k v_k^2}{l_k} \int_0^1 \xi \left(\sum_{i=1}^{N} \kappa'_{ki}\kappa_{kj} \right) d\xi \\ &\quad - \frac{\rho_k v_k^2}{l_k} \int_0^1 (1-\xi)^2 \sum_{i=1}^{N} \kappa'_{ki}\kappa'_{ki} d\xi \\ &\quad + \int_0^1 \left(\frac{T_k(\xi,t)}{l_k} \sum_{i=1}^{N} \kappa'_{ki}\kappa'_{ki} \right) d\xi \\ &\quad + \frac{EA}{2l_k^3} \int_0^1 \left(3\widehat{h}_{ky,\xi}^2 + \widehat{h}_{kw,\xi}^2 \right) \sum_{i=1}^{N} \kappa'_{ki}\kappa'_{ki} d\xi \\ &\quad - \zeta_k \rho_k v_k \int_0^1 \xi \left(\sum_{i=1}^{N} \kappa'_{ki}(\xi)\kappa_{kj} \right) r_{ki}(t) d\xi, \end{aligned} \tag{C.4}$$

$$\begin{aligned} F_{u_k,j} &= \left[\rho_k (g - a_k) l_k - \rho_k v_k^2 \right] \int_0^1 \phi_{kj} dx \\ &\quad + \rho_k v_k^2 \int_0^1 (1-\xi)\phi'_{kj} d\xi - \int_0^1 T_k(\xi,t)\phi'_{kj} d\xi, \\ F_{y_k,j} &= -\Bigg(\rho_k l_k \int_0^1 \widehat{h}_{ky,tt}\kappa_{kj} d\xi + \rho_k a_k \int_0^1 (1-\xi)\widehat{h}_{ky,\xi}\kappa_{kj} d\xi \\ &\quad + \frac{\rho_k v_k^2}{l_k} \int_0^1 \xi \widehat{h}_{ky,\xi}\kappa_{kj} d\xi \\ &\quad + \rho_k v_k \int_0^1 \left[\widehat{h}_{ky,t} + (1-\xi)\widehat{h}_{ky,\xi t} \right] \kappa_{kj} d\xi \\ &\quad - \rho_k v_k \int_0^1 (1-\xi)\widehat{h}_{ky,t}\kappa'_{kj} dl\xi \\ &\quad + \int_0^1 \left(\frac{T_k(\xi,t)}{l_k} \widehat{h}_{ky,\xi}\kappa'_{kj} \right) d\xi \Bigg), \\ F_{u_c} &= m_c(g - a), \\ F_{y_c} &= 0, \end{aligned} \tag{C.5}$$

$$N_{u_i} = -\frac{EA}{2l_i^2} \int_0^1 \left(\phi'_{ij}(\xi) \mathbf{R}_i^{\mathrm{T}} \mathbf{K}_i'^{\mathrm{T}} \mathbf{K}'_i \mathbf{R}_i \right) d\xi, \tag{C.6}$$

$$\begin{aligned} N_{y_i} &= -\int_0^1 \Bigg(\frac{\mathrm{EA}}{l_i^3} \left(\mathbf{q}_i^{\mathrm{T}} \boldsymbol{\Phi}_i'^{\mathrm{T}} \mathbf{K}'_i \mathbf{R}_i \right) \kappa'_{ij} \\ &\quad + \frac{EA}{2l_i^3} \kappa'_{ij} \Big[\Big(\mathbf{R}_i^{\mathrm{T}} \mathbf{K}_i'^{\mathrm{T}} \mathbf{K}'_i \mathbf{R}_i \mathbf{K}'_i \mathbf{R}_i \\ &\quad + 3\widehat{h}_{iy,\xi} \mathbf{R}_i^{\mathrm{T}} \mathbf{K}_i'^{\mathrm{T}} \mathbf{K}_i^{\mathrm{T}} \mathbf{R}_i \Big) \Big] \Bigg) d\xi, \end{aligned} \tag{C.7}$$

where $\mathbf{K}_i = [\kappa_{i1}, \ldots, \kappa_{iN}], \mathbf{R}_i = [r_{i1}, \ldots, r_{iN}], \boldsymbol{\Phi}_i = [\phi_{i1}, \phi_{i2}, \ldots, \phi_{iN}], \mathbf{q}_i = [q_{i1}, q_{i2}, \ldots, q_{iN}]$.

Data Availability

The data used to support the findings of this study are available from the corresponding author upon request.

Conflicts of Interest

The authors declare that there are no conflicts of interest regarding the publication of this paper.

Acknowledgments

This work was supported by the National Key Research and Development Program (2016YFC0600901) and the Priority Academic Program Development of Jiangsu Higher Education Institutions (PAPD), China.

References

[1] S. Qian, B. Zi, D. Zhang, and L. Zhang, "Kinematics and error analysis of cooperative cable parallel manipulators for

multiple mobile cranes," *International Journal of Mechanics and Materials in Design*, vol. 10, no. 4, pp. 395–409, 2014.

[2] X. Arrasate, S. Kaczmarczyk, G. Almandoz, J. M. Abete, and I. Isasa, "The modelling, simulation and experimental testing of the dynamic responses of an elevator system," *Mechanical Systems & Signal Processing*, vol. 42, no. 1-2, pp. 258–282, 2014.

[3] D. Wang, D. Zhang, and S. Ge, "Effect of terminal mass on fretting and fatigue parameters of a hoisting rope during a lifting cycle in coal mine," *Engineering Failure Analysis*, vol. 36, no. 1, pp. 407–422, 2014.

[4] H. Kimura, Z. Min, T. Ishii, A. Yamamoto, and H. Shiba, "Vibration analysis of elevator rope (simplified calculation method for detecting rope deflection of moving cage during earthquake)," *Transactions of the Japan Society of Mechanical Engineers Series C*, vol. 77, no. 773, pp. 43–50, 2011.

[5] S. Kaczmarczyk and W. Ostachowicz, "Transient vibration phenomena in deep mine hoisting cables. Part 1: mathematical model," *Journal of Sound and Vibration*, vol. 262, no. 2, pp. 219–244, 2003.

[6] S. Kaczmarczyk and P. Picton, "The prediction of nonlinear responses and active stiffness control of moving slender continua subjected to dynamic loadings in vertical host structures," *International Journal of Acoustics & Vibrations*, vol. 4, no. 1, pp. 2767–2774, 2011.

[7] H. Ren and W. D. Zhu, "An accurate spatial discretization and substructure method with application to moving elevator cable-car systems—part II: application," *Journal of Vibration and Acoustics*, vol. 135, no. 5, article 051037, 2013.

[8] W. D. Zhu and H. Ren, "An accurate spatial discretization and substructure method with application to moving elevator cable-car systems—Part I: methodology," *Journal of Vibration and Acoustics*, vol. 135, no. 5, article 051036, 2013.

[9] J. H. Bao, P. Zhang, and C. M. Zhu, "Modeling and control of longitudinal vibration on flexible hoisting systems with time-varying length," *Procedia Engineering*, vol. 15, pp. 4521–4526, 2011.

[10] P.-H. Wang, R.-F. Fung, and M.-J. Lee, "Finite element analysis of a three-dimensional underwater cable with time-dependent length," *Journal of Sound and Vibration*, vol. 209, no. 2, pp. 223–249, 1998.

[11] Y. D. Wang, G. H. Cao, Z. C. Zhu, J. J. Wang, and N. G. Wang, "Longitudinal response of parallel hoisting system with time-varying rope length," *Journal of Vibroengineering*, vol. 16, no. 8, pp. 4088–4101, 2014.

[12] K. Yang, "Swing and sloshing of container on guiding rope device," *Journal of Beijing Iron and Steel Institute*, vol. 1986, no. 4, pp. 115–119, 1986.

[13] K. Yang, "Swing of container on guiding rope device when sudden braking," *Mining & Processing Equipment*, vol. 1984, no. 8, pp. 24–26, 1984.

[14] Y. Sai, "Cause analysis of horizontal swing of lifting bucket," *Hrbei Coal*, vol. 1992, no. 3, pp. 136–138, 1992.

[15] Y. Sai, "Dynamic analysis of influence of oscillation of hoist rope on bucket oscillation," *Journal of Xi'an University of Science and Technology*, vol. 2000, no. 1, pp. 9–13, 2000.

[16] Y. Sai and K. Yang, "Further analysis of swing of single-rope lifting container on guiding rope device," *Journal of Xi'an Mining Institute*, vol. 1991, no. 1, pp. 59–66, 1991.

[17] G. H. Cao, J. J. Wang, and Z. C. Zhu, "Coupled vibrations of rope-guided hoisting system with tension difference between two guiding ropes," *Proceedings of the Institution of Mechanical Engineers Part C Journal of Mechanical Engineering Science*, vol. 232, no. 2, pp. 231–244, 2018.

[18] J. J. Wang, G. H. Cao, and Z. C. Zhu, "Lateral and torsional vibrations of cable-guided hoisting system with eccentric load," *Journal of Vibroengineering*, vol. 18, no. 6, pp. 3524–3538, 2016.

[19] N. G. Wang, G. H. Cao, L. Yan, and L. Wang, "Modeling and control for a multi-rope parallel suspension lifting system under spatial distributed tensions and multiple constraints," *Symmetry*, vol. 10, no. 9, pp. 1–24, 2018.

[20] R. S. Crespo, S. Kaczmarczyk, P. Picton, and H. Su, "Modelling and simulation of a stationary high-rise elevator system to predict the dynamic interactions between its components," *International Journal of Mechanical Sciences*, vol. 137, pp. 24–45, 2018.

[21] M. Otsuki, Y. Ushijima, K. Yoshida, H. Kimura, and T. Nakagawa, "Application of nonstationary sliding mode control to suppression of transverse vibration of elevator rope using input device with gaps," *JSME International Journal Series C*, vol. 49, no. 2, pp. 385–394, 2006.

[22] J. H. Bao, P. Zhang, C. M. Zhu, M. Zhu, L. Q. Jin, and H. X. Xie, "Vibration control of high-speed elevator hoisting systems based on tensioning devices," *Journal of Vibration & Shock*, vol. 36, no. 14, pp. 221–226, 2017.

[23] H. Ren, *Accurate Simulation of the Dynamics of Elevator Systems*, University of Maryland, Baltimore County, MD, USA, 2011.

[24] J. Wu, Z. M. Kou, and M. Liang, "Transverse dynamics analysis of rope in multi-rope friction hoisting system," *Journal of Vibration and Shock*, vol. 35, no. 2, pp. 184–188, 2016.

[25] A. Kumaniecka and J. Nizioł, "Dynamic stability of a rope with slow variability of the parameters," *Journal of Sound and Vibration*, vol. 178, no. 2, pp. 211–226, 1994.